



HAL
open science

Photogeneration of Several Linkage Isomers and Investigation of Forward and Backward Nitro-Nitrito Isomerization Processes in a Palladium Complex

Artem Mikhailov, Krzysztof Konieczny, Maria Gladysheva, Pavel Plyusnin, Sébastien Pillet, Dominik Schaniel

► **To cite this version:**

Artem Mikhailov, Krzysztof Konieczny, Maria Gladysheva, Pavel Plyusnin, Sébastien Pillet, et al.. Photogeneration of Several Linkage Isomers and Investigation of Forward and Backward Nitro-Nitrito Isomerization Processes in a Palladium Complex. *Inorganic Chemistry*, 2023, 62 (14), pp.5531-5542. 10.1021/acs.inorgchem.3c00028 . hal-04067273

HAL Id: hal-04067273

<https://hal.univ-lorraine.fr/hal-04067273v1>

Submitted on 13 Apr 2023

HAL is a multi-disciplinary open access archive for the deposit and dissemination of scientific research documents, whether they are published or not. The documents may come from teaching and research institutions in France or abroad, or from public or private research centers.

L'archive ouverte pluridisciplinaire **HAL**, est destinée au dépôt et à la diffusion de documents scientifiques de niveau recherche, publiés ou non, émanant des établissements d'enseignement et de recherche français ou étrangers, des laboratoires publics ou privés.

Photogeneration of several linkage isomers and investigation of forward and backward nitro-nitrito isomerization processes in a palladium complex

Artem Mikhailov^{a*}, Krzysztof A. Konieczny^{a,b}, Maria Gladysheva^{c,d}, Pavel Plyusnin^c, Sébastien Pillet^a, Dominik Schaniel^a

*Corresponding author: artem.mikhailov.a@gmail.com

^a Université de Lorraine, CNRS, CRM2, UMR 7036, Nancy 54000, France

^b Institute of Advanced Materials, Wrocław University of Science and Technology, Wybrzeże Wyspiańskiego 27, 50-370 Wrocław, Poland

^c Nikolaev Institute of Inorganic Chemistry, Siberian Branch of the Russian Academy of Sciences, 3 Acad. Lavrentiev Avenue, Novosibirsk 630090, Russian Federation

^d Novosibirsk State University, Pirogova 1, Novosibirsk 630090, Russian Federation

Abstract

Photoinduced linkage isomers (PLIs) of the nitro-ligand were generated and comprehensively characterized in a square planar unit $[\text{Pd}(\text{NH}_3)_3\text{NO}_2]^+$ of the complex salts $[\text{Pd}(\text{NH}_3)_4][\text{Pd}(\text{NH}_3)_3\text{NO}_2][\text{MOx}_3] \cdot \gamma\text{H}_2\text{O}$ ($\text{M} = \text{Cr}$ (**Cr**), Rh (**Rh**), Co (**Co**), $\text{Ox} = \text{oxalate}$). The structural (XRD) and spectroscopic (IR, UV-vis) investigations at 10 and 150 K allowed to determine the structures of several photoinduced linkage isomers, *endo*-ONO (PLI1, 2) and *exo*-ONO (PLI3, 4) isomers generated by irradiation with 365 nm from the initial NO_2 (GS), along with the assignment of the IR-bands to each structural isomer. Based on a combination of these methods the photo- and thermally induced interplay of PLIs was investigated. Irradiation in the temperature range 10-80 K induces the formation of both *endo*- and *exo*-ONO isomers, while increasing the temperature up to 150 K results in the formation of only *endo*-ONO isomers. The structural arrangement of the *endo*-ONO and *exo*-ONO PLI is strongly influenced by intermolecular interactions due the partial occupation of a neighboring site by water molecules. The investigation of thermal dynamics of PLIs revealed that the thermal decay of the *exo*-ONO isomer occurs via two steps $\text{exo-ONO} \rightarrow \text{endo-ONO} \rightarrow \text{NO}_2$. The kinetic parameters (E_a , k_0) of both decay processes were determined together with the characteristic decay temperatures (T_d) by IR-spectroscopy. According to the photoinduced dynamics measured by IR-spectroscopy, the mechanism of PLIs formation in $[\text{Pd}(\text{NH}_3)_3\text{NO}_2]^+$ could be described as $\text{NO}_2 \rightarrow \text{endo-ONO} \rightarrow \text{exo-ONO}$.

Introduction

The ability of a ligand to change its conformation under an external stimulus such as electric field, pH value or light irradiation has attracted a lot of attention in the last decades. For example, the works by J.P. Sauvage, J. F. Stoddart and B. L. Feringa on molecular machines were honored by the Nobel Prize in 2016.^{1,2} There exist various families of switchable ligands in coordination compounds, amongst which the nitro-ligand NO_2^- that can undergo photoinduced isomerization $\text{M-NO}_2 \rightarrow \text{M-ONO}$ ($\text{M} = \text{metal}$).³ Moreover, depending on the nature of the complex and the experimental conditions, the nitrito isomer ONO can be stabilized in several configurations, such as *endo*-ONO, *exo*-ONO or $\kappa^2\text{-O,O-(ONO)}$.⁴⁻⁸

Photoinduced linkage isomers (PLIs) of the nitrite ligand can be generated by light with different wavelengths in the range of 350-650 nm.^{7,9,10} In general, in these systems a backward reaction $\text{M-ONO} \rightarrow \text{M-NO}_2$ is accessible only by heating, *i.e.* nitrito PLIs are metastable states, however, there are two examples of partial light induced backward reaction in case of $[\text{Co}(\text{Me-dpt})(\text{NO}_2)_3]$ ($\text{Me-dpt} = 3,3'$ -diamino-N-methylpropanediamine) and ruthenium complex *trans*- $[\text{Ru}(\text{py})_4(\text{NO}_2)_2]$ ($\text{py} = \text{pyridine}$).^{11,12} The degree of metastability is governed by the height of the activation barrier,¹³⁻¹⁵ and in practice the majority of nitrito PLIs are stable at temperatures below

300 K.^{5,16,17} Nevertheless, there are several examples of complexes exhibiting much higher thermal stability at room temperature, such as mentioned above cobalt complex or platinum compound *trans*-[Pt(PCy₃)₂(NO₂)₂] (PCy₃ = tricyclohexylphosphine).^{11,16} The forward nitro-nitrito isomerization might be thermally induced at high temperature (\approx 400 K) as well, which was shown for nickel complexes.^{18,19}

The isomerization process is sensitive to the nearest surrounding of the NO₂ ligand. The reaction cavity shape and volume available for the nitro-nitrito ligand influence significantly the conversion of the M-NO₂ \rightarrow M-ONO reaction.^{20,21} For instance, in the [Pt(NO₂)₄]²⁻ complex the population of the *endo*-ONO isomers is varied for each ligand in the range of 0-65% depending on the size of the cavity around NO₂ (from 0.95 to 3.40 Å³).²⁰ The presence of a hydrogen bond between H-donor and NO₂ ligand also influences the population of PLIs.²² It was shown that the presence of hydrogen bonds can lead to a reduction of the population of PLI, and that the hydrogen bond lengths can be manipulated by temperature. As a result, higher population of PLIs are observed at higher temperatures (around 150 K) compared to the ones obtained at 100 K.

Quantum chemical calculations suggest that the mechanism of the nitro-nitrito isomerization in octahedral complexes consists of two stages NO₂ \rightarrow *endo*-ONO \rightarrow *exo*-ONO.¹³⁻¹⁵ Although the structures of *endo*- and *exo*-isomers were reported for different square planar and octahedral compounds,^{5,16,17} up to date there are no systematic experimental reports on the mechanism of the photoisomerization. This might be related to several restrictions: not every compound exhibits the formation of both *endo*- and *exo*-isomers due to the limitations induced by the reaction cavity around NO₂, the absorption properties of the complex or the stability of the crystal against light irradiation³, and temperatures below 80 K may be required to stabilize PLIs.

The classic octahedral nitro complex [Co(NH₃)₅NO₂]²⁺ is the subject of investigation since more than 100 years.²³⁻²⁶ The simple ligand composition of the complex allowed to investigate its nitro-nitrito isomerization experimentally and theoretically.^{15,27} However, according to the Cambridge Crystallographic Data Centre (CCDC) there are no known structures of square planar complexes with formula {M(NH₃)₃NO₂}. In the Inorganic Crystal Structure Database (ICSD) only one related structure [Pd(NH₃)₃(NO₂)] [Rh(NH₃)₂(NO₂)₄] was found.²⁸ Unfortunately, the pure bulk phase of the complex was not reported. Compounds with such formula could be convenient species for the theoretical modeling of nitro-nitrito isomerization in square planar compounds, as well as for the experimental investigation of possible PLIs.

Recently, a series of isostructural compounds with formula [Pd(NH₃)₄][Pd(NH₃)₃NO₂][MOx₃] \cdot yH₂O (M = Cr (**Cr**), Rh (**Rh**), Co (**Co**), Ox = oxalate) was synthesized for the preparation of catalytic systems.^{29,30} Interestingly, up to date the complex [Pd(NH₃)₃NO₂]⁺ could only be stabilized in such complex salt. Since, in the series of the compounds the anionic part [MOx₃]³⁻ differs, there is a possibility to investigate the influence of the anion on the properties of PLIs in [Pd(NH₃)₃NO₂]⁺. Our current report is devoted to the experimental investigation of PLIs in [Pd(NH₃)₃NO₂]⁺, especially to the study of forward - photoinduced and backward - thermally induced processes of nitro-nitrito isomerization.

Experimental

Synthesis

The compounds of general summary formula [Pd(NH₃)₄][Pd(NH₃)₃NO₂][MOx₃] \cdot yH₂O (M = Cr (**Cr**), Rh (**Rh**), Co (**Co**), Ox = oxalate) were synthesized according to the previously published procedure.^{29,30}

SCXRD

The X-ray data were collected on Rigaku Supernova diffractometer with Excalibur CCD detector using microfocus MoK α X-ray source (λ = 0.71073 Å). CrysAlisPro (ver. 1.171.41.93a) software package was used both for data collection and reduction.³¹ The low temperature during measurements was obtained using liquid nitrogen at 150 K and liquid helium at 10 K.

The crystal structures of ground states (GS) and photoinduced linkage isomers (PLIs) were solved using ShelXT.³² All structures were refined by means of ShelXL³³ implemented in Olex2.³⁴ The disorder in photoexcited crystals was refined based on Fourier difference map of given structure and photodifference map calculated between respective PLI and GS observed structure factors ($F_{\text{obsPLI}} - F_{\text{obsGS}}$).³⁵ The atoms were named according to the labels given in Fig. 1 and 2. The structures of the disordered fragments in the determined structures are presented in Fig. 2 with corresponding photodifference maps in the plane of the nitro group in Fig. S1. The Pd-N/O distances for all observed NO₂/ONO forms are gathered in Table 1. In all crystal structures all non-hydrogen atoms were refined anisotropically, except for the **Cr** structure measured at 10 K after light excitation where NO₂/ONO disorder was refined over 5 occupation sites, in which minor components were refined isotropically. The hydrogen atoms positions in NH₃ groups were constrained and treated as riding rotating groups. Water molecules were treated as rigid groups, with positions of hydrogen atoms deduced from hydrogen bonds. In disordered crystal structures a set of restraints on bond lengths, valence angles and ADP's were applied, adjusted individually for each structure, but in an analogous manner within a measurement's series. In disordered structures the atoms N1, O1 and O2 forming ONO were additionally labeled with suffixes "A" (PLI1), "B" (PLI2), "C" (PLI3) and "D" (PLI4) depending on the conformation of PLI (see Fig. 2).

Selected crystallographic data are gathered in Table S1. CCDC numbers 2191057-2191064 for **Co** (150 K, GS), **Co** (150 K, GS+PLI1, 2), **Cr** (10 K, GS), **Cr** (150 K, GS), **Cr** (10 K, GS+PLI1, 2, 3, 4), **Cr** (150 K, GS+PLI1, 2), **Rh** (150 K, GS), **Rh** (150 K, GS+PLI1, 2), respectively, contain the supplementary crystallographic data for this paper. These data can be obtained free of charge from The Cambridge Crystallographic Data Centre via www.ccdc.cam.ac.uk/structures.

All single crystal irradiations were performed in-situ on the diffractometer by means of 365 nm Thorlabs LED (Light Emitting Diodes) with 150 mW optical power. All crystals studied at 150 K were irradiated for 60 min. Additionally, the crystal of **Rh** was irradiated for another 180 min (240 min in total). **Cr** crystal at 10 K was irradiated for 30 min. During irradiation the crystals were rotated constantly around the axis perpendicular to the light beam to ensure a homogenous distribution of the photoproduct in the whole crystal volume. After each irradiation time the XRD experiment was performed and the crystal structure was determined. Additionally, all structures were measured after thermal relaxation of PLIs to confirm the relaxation of PLIs back to GS.

IR- and UV-vis-spectroscopy

IR-spectroscopy measurements with irradiation were performed using a Nicolet 5700 FT-IR spectrometer with a resolution of 2 cm⁻¹ in the range 400–4000 cm⁻¹. The sample (around 1-2 mg) was mixed with KBr (around 100 mg) and pressed into common pellets for IR measurements. The pellets were bonded onto the cold finger of a closed-cycle cryostat (Oxford Optistat) allowing to control the temperature in the range 10 - 300 K. The irradiation procedures were performed by Thorlabs LEDs through KBr windows perpendicular to the samples with light of different wavelengths (365 – 660 nm) with 50 - 200 mW optical power. The highest population of PLIs was achieved by using 365 nm LED for all compounds. The assignment of IR bands of PLIs was made based on the populations of PLIs obtained from the XRD data measured at 150 and 10 K. The photogeneration of PLIs at 150 K results in the formation of endo-isomers PLI1, 2, while the photogeneration at 10 K additionally leads to the formation of exo-isomers PLI3, 4 (PLI4 was not directly observed in IR). Importantly, the populations of PLI1, 2 determined by XRD, and relative band intensities of PLI1, 2 measured by IR show the same trend for all three investigated compounds (higher population of PLI1 from XRD corresponds to higher band intensity of PLI1 from IR). The IR measurements performed at different temperatures confirm these assignments and allow following the evolution of the spectra: for example, thermal decay of PLI3 to PLI1 reveals the decrease of PLI3 bands, the increase of PLI1 bands and no intensity change in case of PLI2. To investigate the isothermal kinetics during the decay of PLIs the following protocol was applied: on the first stage the sample was irradiated at 150 or 10 K by 365 nm light in order to generate a sufficient amount of PLI; then the temperature was increased up to a chosen value (90-110 K for PLI3 and 230-250 K in case of PLI1, 2) and then repeated measurements (the delay between spectra was about 60s) was performed in isothermal mode. The decay constants were calculated

from the decrease of the intensity of the maximum of $\nu^s(\text{ONO})$ band of PLI1-3 in the range 1000-1100 cm^{-1} . The obtained experimental data were approximated using the equation of a first-order decay $A=A_0 \cdot \exp(-k \cdot t) + A_\infty$. Further, using the decay constants (k) determined at each measured temperature (T), the activation energy (E_a) and frequency factor (k_0) were determined in Arrhenius coordinates ($k=k_0 \cdot \exp(-E_a/(R \cdot T))$, R - molar gas constant).

UV-vis spectra were recorded using transparent KBr pellets with the embedded complex on a Varian CARY 4000 spectrometer. The transparent pellets were prepared and irradiated as for the IR measurements. Low-temperature measurements were performed using the same cryostat as that for the IR measurements, except that the KBr windows were exchanged for standard borosilicate glass windows. The baseline was measured using the same diaphragm with a KBr pellet, which can be mounted on the cryostat sample holder.

Results and discussion

SCXRD

All determined crystal structures are isostructural, regardless of the central atom (M) in the oxalate part $[\text{MOx}_3]^{3-}$. The asymmetric unit in GS at 10 K is shown on the example of **Cr** in Fig. 1. The composition of the crystals is as follows: $[\text{Pd}(\text{NH}_3)_4][\text{Pd}(\text{NH}_3)_3\text{NO}_2][\text{MOx}_3] \cdot \gamma \text{H}_2\text{O}$, where $M = \text{Cr}$ (**Cr**), Rh (**Rh**) or Co (**Co**). The water content was approximately the same for all crystals, $\gamma \approx 0.7$, except for the crystal of **Cr** measured at 10 K for which $\gamma \approx 0.5$, since these measurements with the use of liquid helium were conducted a few weeks after data collection at 150 K that resulted in water loss in the crystal due to evaporation over time. In all investigated compounds the solvate water molecule is in the vicinity of the NO_2 ligand with the donor-acceptor distance $\text{O3}(\text{H}_2\text{O}) \cdots \text{O2}(\text{NO}_2)$ of about 2.7 Å (Fig. 2, *a*). Since the occupancy of the H_2O site is about 0.7 (or 0.5 in case of **Cr** structure measured at 10 K), there are 70% (or 50%) of NO_2 ligands with the H_2O molecule in the nearest environment, while the remaining 30% (or 50%) of NO_2 are sites without neighboring solvent H_2O . This fact strongly influences the formation of linkage isomers in the investigated compounds, as discussed below.

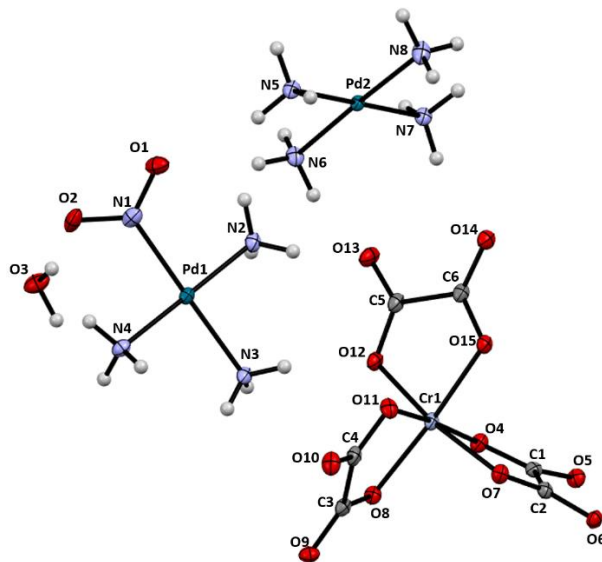


Fig. 1. Asymmetric unit of **Cr** at 10 K. Atomic displacement parameters are drawn at 50% probability level. ³⁶

Irradiation at 150 and 10 K

The irradiation (light of wavelength 365 nm) of single-crystals at different temperatures leads to different observations. Irradiation at 150 K leads to the photoisomerization of GS nitro groups (NO_2) to *endo*-ONO nitrito groups having two possible conformations (photoproducts "A" (PLI1) and "B" (PLI2)) (see Figs. 2, S2). The structural difference between *endo*-ONO isomers PLI1 and PLI2 is shown in detail in Fig. 2, *b-d*. Due to the partial

occupancy of solvate H₂O molecules (about 0.7), two types of the *endo*-ONO isomers are formed after light irradiation of GS. For the [Pd(NH₃)₃NO₂]⁺ molecules where H₂O is present (70%) the light excitation of GS leads to the formation of PLI1 (Fig. 2, c), whereas the sites without water (the remaining 30%) in the vicinity of [Pd(NH₃)₃NO₂]⁺ form PLI2, as shown in Fig. 2, d. Generally, the formation of PLI2 is sterically impossible if there is a water molecule nearby, since the intermolecular distance O3(H₂O)⋯O2B(ONO) in that case would be 1.4 Å (see Fig. 2, b), and would be even shorter in case of O3-H(H₂O)⋯O2B(ONO) contact (about 0.6 Å). Structurally, the isomers PLI1 and PLI2 in case of **Cr**, **Rh** and **Co** are almost identical (see Table 1), the corresponding representative structural models obtained for **Cr** are shown in Fig. 2, a-d.

In the crystal of **Cr** studied at 10 K two more *exo*-ONO nitrito groups of two conformations (photoproducts “C” (PLI3) and “D” (PLI4)) were detected (see Fig. 2, e, f and Fig. S2), which are stable below 80 K. Similar to PLI1 and PLI2, the *exo*-ONO isomer PLI3 is found in the case with a nearby water molecule, whereas PLI4 is related to the [Pd(NH₃)₃NO₂]⁺ without H₂O in the closest environment. The Pd-N/O distances and populations of all isomers within the studied crystals, based on *site occupation factors* from determined X-ray structures, are gathered in Tables 1 and 2.

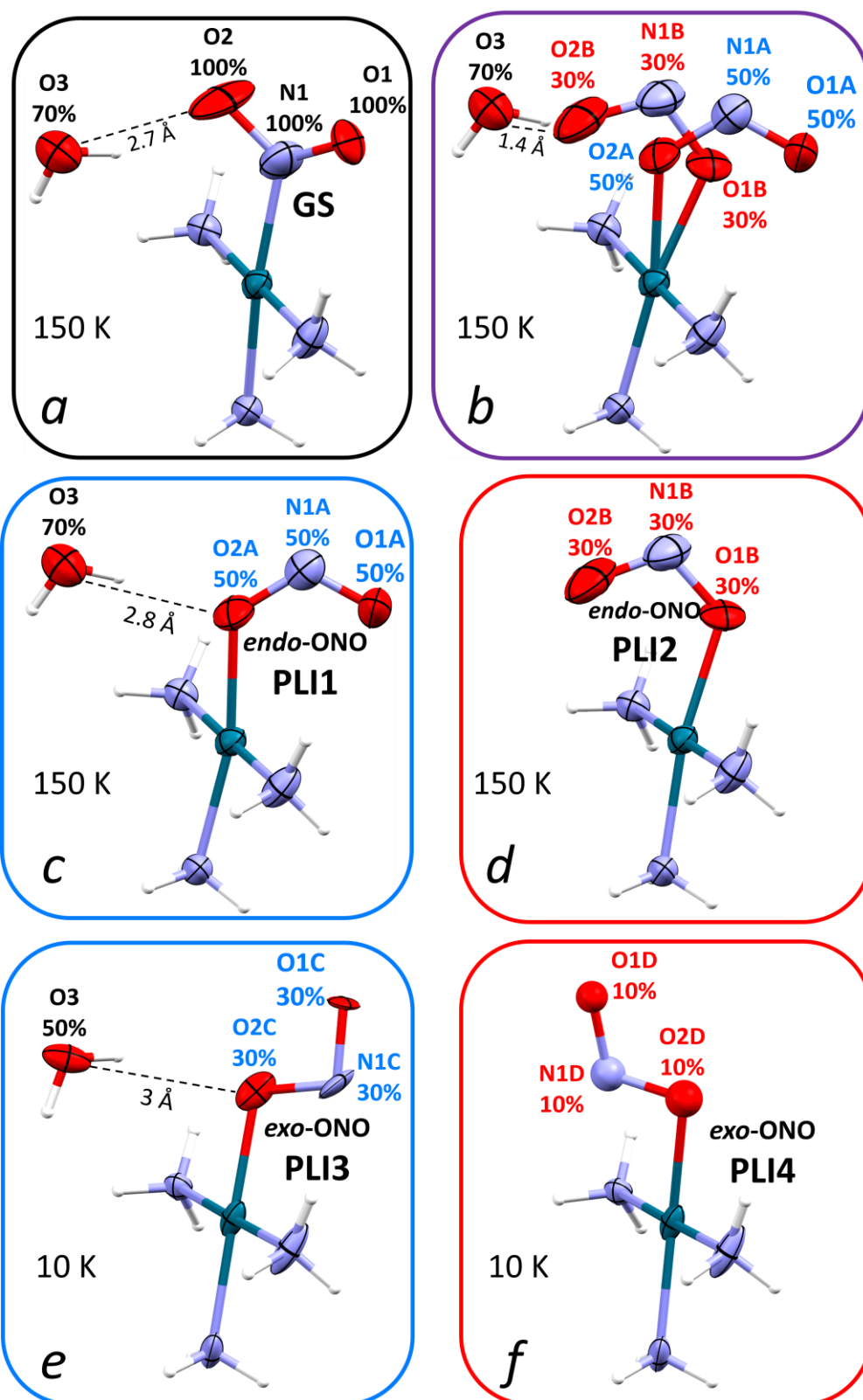


Fig. 2. The photoswitchable fragment $[\text{Pd}(\text{NH}_3)_3\text{NO}_2]^+ / [\text{Pd}(\text{NH}_3)_3\text{ONO}]^+$ in the structure of **Cr**. Panel *a*: the fragment $[\text{Pd}(\text{NH}_3)_3\text{NO}_2]^+$ (GS) with depicted intermolecular contact with H_2O , the structure is measured at 150 K; panel *b*: the structures of *endo*-ONO isomers PLI1 and PLI2 in $[\text{Pd}(\text{NH}_3)_3\text{ONO}]^+$ measured at 150 K after 365 nm irradiation, GS part (NO_2) is omitted for clarity; panel *c*: the *endo*-ONO PLI1 isomer having H_2O molecule in the nearest surrounding, GS and PLI2 parts are omitted for clarity; panel *d*: the *endo*-ONO PLI2 isomer, which does not have H_2O molecule in the vicinity, GS and PLI1 parts are omitted for clarity; panel *e*: the structure of *exo*-ONO isomer PLI3 in $[\text{Pd}(\text{NH}_3)_3\text{ONO}]^+$ measured from another crystal at 10 K after 365 nm irradiation, GS,

PLI1, PLI2 and PLI4 parts are omitted for clarity; panel *f*: the structure of *exo*-ONO isomer PLI4 in $[\text{Pd}(\text{NH}_3)_3\text{ONO}]^+$ measured from another crystal at 10 K after 365 nm irradiation, GS, PLI1, PLI2 and PLI3 parts are omitted for clarity.

Comparison of crystals measured at 150 K shows that the highest population of *endo*-ONO occurs for **Cr** (82.6% of products in total) and the lowest for **Rh** (29.3% of products in total) even though the **Rh** single crystal was irradiated 4 times longer. This is most probably due to the limited light penetration depth,³⁷ since the crystal of **Rh** was significantly bigger (0.012 mm^3 for **Cr** vs 0.030 mm^3 for **Rh**). For **Co** 39.9% conversion was observed after 60 min of crystal irradiation, while the crystal size (0.014 mm^3) was comparable to the crystal of **Cr**. Significantly lower population of PLIs in this case could be possibly related to the sample degradation over irradiation time due to CO_2 release (see data quality monitoring and IR-spectroscopy parts). Another reason of the different population could be related to a difference in absorption properties of the compounds discussed below in the UV-vis-spectroscopy of PLIs part. The discrepancy in the population however, seems not to be related to the reaction cavity, which is identical for all studied crystals in terms of shape and volume, which is equal to $40(2)$, $39(2)$ and $41(2) \text{ \AA}^3$ for **Cr**, **Co** and **Rh**, respectively (Fig. 3). The void calculations were performed for a spherical volume of 1.0 \AA radius using 0.2 \AA grid.³⁸

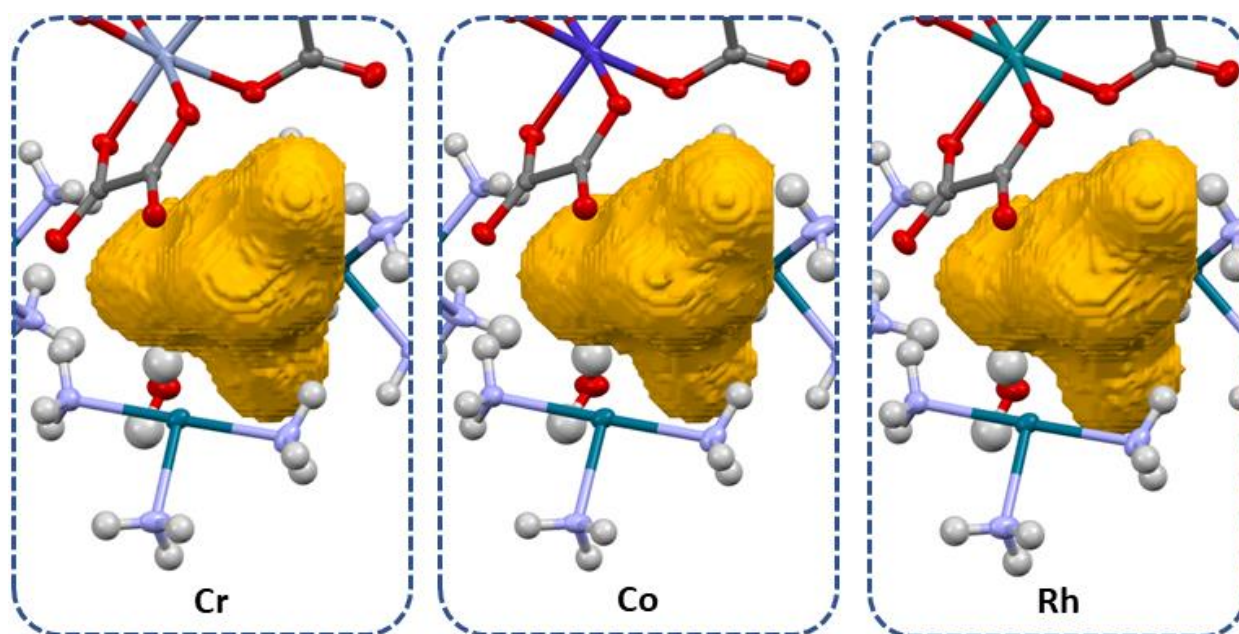


Fig. 3. The reaction cavity expressed as volume occupied by NO_2 group and the void surrounding it using ball of 1.0 \AA radius as a probe with 0.1 \AA grid.³⁶

The investigated compounds offer the possibility to study the influence of hydrogen bonding on the efficiency of the PLI formation, since there is partial occupancy of water molecule. The water molecule plays a key role in the formation of the PLIs through the creation of a $\text{O}_3\text{-H}\cdots\text{O}_2$ hydrogen bond with the nitro group of GS. The donor-acceptor distance in all GS structures is very similar and varies only slightly from $2.727(4)$ to $2.754(4) \text{ \AA}$ (see Table S2). Such a close contact affects photoisomerization in two ways:

- 1) The water molecule is a steric obstacle excluding the formation of *endo*-ONO "B" (PLI2) and *exo*-ONO "D" (PLI4) conformations. Hence, forms "B" (PLI2) and "D" (PLI4) are formed only if there is no water near the reaction center, and the total occupancy of both forms cannot exceed ca. 30% for crystals studied at 150 K and ca. 50% for crystal studied at 10 K, in agreement with data gathered in Table 2, assuming that the occupancy can be determined with an accuracy of 5-6 percentage points. The absence of water molecule results in a relatively large void volume equal to $46(10)$, $47(10)$ and $48(10) \text{ \AA}^3$ for **Cr**, **Co** and **Rh** at 150 K, respectively,

allowing the structural rearrangement of NO₂ during “B” and “D” PLI’s formation (for probe/grid equal to 0.6/0.2Å).

2) Apparently, the conformations “A” (PLI1) and “C” (PLI3) are formed regardless of water presence. Based on the conducted experiments it is hard to determine if the PLI1,3-isomerization is hindered or favored by the hydrogen bond, however it can be assumed that this interaction stabilizes the position of the O2 atom in the nitro group.

Table 1. List of distances between Pd1 and photoreactive ligand (NO₂/ONO).

Complex	T, K	State	Pd1-N1	Pd1-O2A	Pd1-O1B	Pd1-O2C	Pd1-O1D
Co	150	GS	2.000(2)	-	-	-	-
	150	GS, PLI1, 2	2.05(2)	1.95(3)	1.91(7)	-	-
Rh	150	GS	1.997(2)	-	-	-	-
	150	GS, PLI1, 2	2.03(1)	1.98(3)	1.88(9)	-	-
Cr	150	GS	1.995(2)	-	-	-	-
	150	GS, PLI1, 2	1.965(9)	2.028(5)	2.007(6)	-	-
	10	GS	1.999(2)	-	-	-	-
	10	GS, PLI1, 2, 3, 4	1.981(6)	2.05(1)	2.06(2)	1.981(6)	2.03(2)

Table 2. Products’ content in photoexcited structures.

Complex	T, K	Component occupancy [%]				
		GS NO ₂	PLI1 "A" <i>endo</i> -ONO	PLI2 "B" <i>endo</i> -ONO	PLI3 "C" <i>exo</i> -ONO	PLI4 "D" <i>exo</i> -ONO
Co	150	60.1	21.7	18.2	-	-
Rh	150	70.7	18.3	11.0	-	-
Cr	150	17.4	48.4	34.2	-	-
	10	39.2	20.8	7.5	26.8	5.8

At first sight the presence of both “A” (PLI1) and “B” (PLI2) *endo*-conformations suggests that the formation of “B” (PLI2) is favorable, and “A” (PLI1) occurs only if there is a water molecule near the reaction center. Indeed, in case of **Cr** crystal studied at 150 K, the conformation “B” (PLI2) is formed whenever it is possible (for ca. 70% water occupancy ca. 30% of “B” (PLI2) was formed). However, at 10 K the total amount of forms “B” (PLI2) and “D” (PLI4) is equal to ca. 13%, even though the water occupies only half of the whole reaction centers, whilst forms “A” (PLI1) and “C” (PLI3) together occupy almost 50% of molecules (see Table 2). The directionality of the photoisomerization depends then, not only on water presence/absence but the temperature at which light excitation occurs setting up the photochemical equilibrium between all isomers and allowing the formation of the less stable *exo*-isomers PLI3, 4. The reaction route also might be tuned by the closest environment of the photoswitchable ligand, which is variable in function of temperature^{3,8,17,39} and product content,⁴⁰⁻⁴³ however, in current case no significant differences are observed between GS structures measured at 10 and 150 K (Table 1, S2).

Thus, the XRD measurements at 150 and 10 K allowed to determine the structures of four PLIs denoted as PLI1, 2 (*endo*-ONO) and PLI 3, 4 (*exo*-ONO). The information on the relative populations of PLIs and their thermal

stability allowed to unambiguously assign the vibrational bands discussed below in the IR-spectroscopy section to the corresponding linkage isomer.

Data quality monitoring

The photoexcitation may have additional effects affecting crystal quality, such as crystal damage caused by internal stresses due to potentially significant displacements of atoms during photoisomerization. This can be prevented if the molecular movement during the reaction is relatively small and the atoms forming photoproduct occupy similar positions in a crystal, if there is a lot of free space around reaction center and/or if the crystal has a high elasticity.^{3,44} In the studied cases the volume of the unit cell changed after irradiation by 1.3, 1.0, 1.1 and 0.5% for **Cr** at 10 K, **Cr**, **Co** and **Rh** at 150 K, respectively. This relatively small changes suggest rather little strain in the crystals when nitrito isomers are formed.^{3,45} Crystal structures data gathered in Table S1 show that in case of **Cr** and **Rh** the quality of the crystal is maintained during irradiation, *e.g.* for crystal of **Rh** the R_{int} value increased by 0.83 percentage point (from 5.34% to 6.17%) and the number of observed reflections decreased by about 0.65% (from 7502 to 7452 reflections) after irradiation for 240 min. In the case of **Co** however, strong decrease of the crystal quality was observed after crystal irradiation and relaxation back to the ground state, *i.e.* the R_{int} value increased by 8.86 percentage point (from 5.42% through 7.23% after irradiation to 14.28% after relaxation) and the number of observed reflections decreased by 39% (from 7125 through 5526 to 4322 reflections). This effect is related to a CO₂ release from the [CoOx₃]³⁻ part, which is in accordance with IR-spectroscopy data of **Co** (see IR-spectroscopy part).

IR-spectroscopy

Since all the compounds with formula [Pd(NH₃)₄][Pd(NH₃)₃NO₂][MOx₃] (M= Cr (**Cr**), Rh (**Rh**), Co (**Co**)) contain oxalate ligands (Ox), the comparison of IR-spectra of sodium or potassium salts [MOx₃]³⁺ and [Pd(NH₃)₄][Pd(NH₃)₃NO₂][MOx₃] has been done in order to reveal the position of the bands related to the NO₂ ligands. Clearly, the bands at around 1700, 1400, 1250, 900, 800, 600, 550, 480 and 420 cm⁻¹ are characteristic for the vibrations of Ox, as illustrated on the example of **Cr** compound (see Fig. S3). Thus, the known bands of NO₂ ligand at around 1250 and 820 cm⁻¹ are overlapped with those bands and can be observed as several spikes in the range 1250-1300 cm⁻¹ shown in Fig. S3.

Irradiation at 150 K

The irradiation at 150 K with 365 nm light induces similar changes in the IR-spectra of all compounds **Cr**, **Rh** and **Co**. We illustrate the findings on the example of **Cr**, shown in Fig. 4, as it exhibits the highest population. The light excitation leads to a decrease of the intensity of the $\nu(\text{NO}_2)$ bands at 1441 (ν^{as}), 1424_{sh} (ν^{as}), 1338 (ν^{s}), 1309 (ν^{s}) and 1255 (ν^{s}) cm⁻¹ and to the appearance of new bands at 1467 (ν^{as}), 1097 (ν^{s}), 1053 (ν^{s}) cm⁻¹ characteristic for the $\nu(\text{ONO})$ modes.^{8,12,17,26,46,47} Importantly, the intensities of the bands at 1053 and 1097 cm⁻¹ are different and can be used for the estimation of the relative population of PLIs. Based on the populations of PLIs determined by XRD, the bands are assigned to the PLI1 and PLI2, respectively. Moreover, when keeping the KBr pellet with the compound overnight in the cryostat under vacuum, the relative intensities of the bands at 1053 and 1097 cm⁻¹ after light irradiation change (see Fig. S4). This effect is due to the evaporation of the solvent water from the compounds in vacuum, leading to a redistribution of populations of PLI1 and PLI2 (more PLI2 at the cost of PLI1). This observation thus confirms the assignment of these bands and illustrates that the presence (or absence) of intermolecular contacts noticeably influence the population of PLIs in NO₂-compounds.²² After nitro-nitrito photoisomerization other new bands appear at 3406 and 636 cm⁻¹ at 150 K (Fig. 4, S5), which are discussed in detail below. Additionally, the difference spectra before and after generation of PLIs are shown in Fig. S6. The photogeneration of PLIs was probed at different temperatures in the range 10-200 K, the highest population of PLI1 and PLI2 was observed at 150 K, which is consistent with the results reported by Hatcher.²²

It is important to mention that the light excitation at 340, 365, 385, 405, 455, 617 and 660 nm was tested, and the highest population of any PLI was achieved in case of 365 nm. The irradiation at 455, 617 and 660 nm does not induce the photoisomerization reaction.

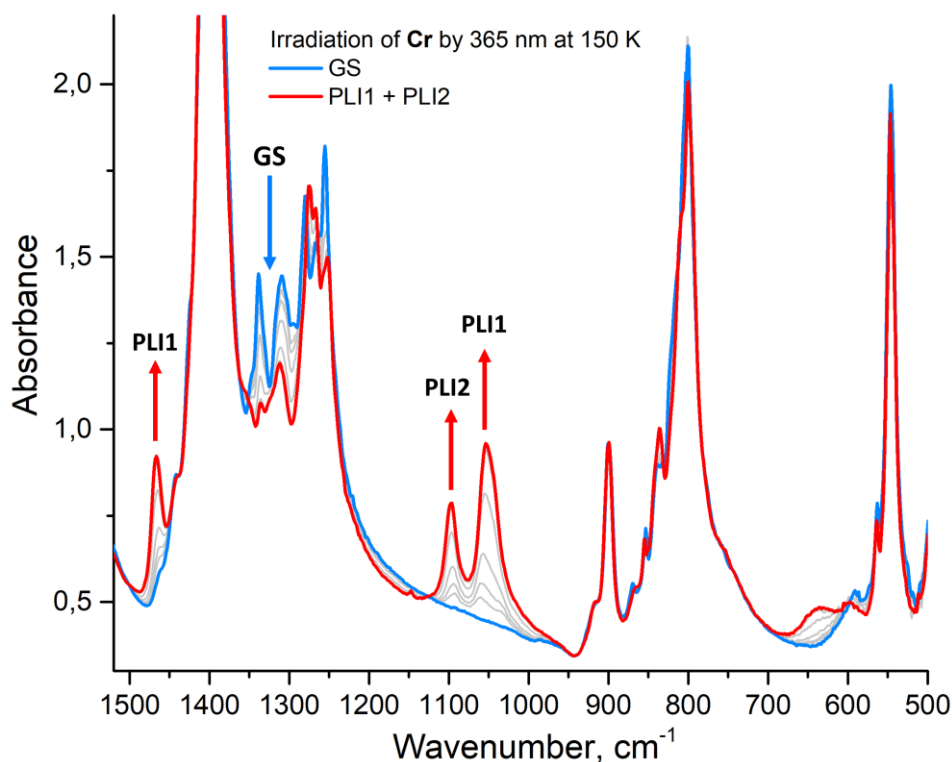


Fig. 4. IR-spectra of **Cr** at 150 K before (GS) and after (PLI1 + PLI2) light irradiation at 365 nm.

Irradiation at 10 K

The irradiation of the complexes at 10 K by the same wavelength (365 nm) leads to the formation of additional new bands in the IR-spectra (see Fig. 5). Besides of PLI1 (1055 cm^{-1}) and PLI2 (1097 cm^{-1}), a band at 1012 (ν^s) cm^{-1} has appeared and is assigned to the $\nu(\text{ONO})$ mode of the PLI3 isomer detected by XRD. Tentatively, a small shoulder at 1000 cm^{-1} could be assigned to PLI4, however due to its low intensity and overlap with other bands, further discussion is limited to PLI1-3. Importantly, the bands $\nu^s(\text{NO}_2)$ provide more complete information on the relative population and dynamics of PLIs compared to $\nu^{as}(\text{NO}_2)$, since they do not overlap with the bands of oxalate ligands. For example, the $\nu^{as}(\text{NO}_2)$ bands of PLI2 at 1440 cm^{-1} appear as low-intensity shoulders (see Table 3).

Based on the photogeneration measurements of PLIs at different temperatures, the main bands of all PLIs at 10 K were assigned and summarized in Table 3. At 10 K the $\nu(\text{NO}_2)$ bands of GS exhibit several spikes, which are better resolved with respect to the spectra at 150 K. Tentatively, on the example of **Cr** compound, the bands at 1445 and 1428 cm^{-1} are assigned to the $\nu^{as}(\text{NO}_2)$ mode, the bands at 1343, 1336, 1311, 1285 and 1258 cm^{-1} reflect the $\nu^s(\text{NO}_2)$ bands. In case of the $\nu(\text{ONO})$ vibrations a larger split of (ν^{as}) and (ν^s) modes occur. Thus, for PLI1-3 the bands (ν^{as}) and (ν^s) are found at 1465 and 1055 cm^{-1} , 1442_{sh} and 1097 cm^{-1} , 1489 and 1012 cm^{-1} , respectively. The $\nu(\text{OH})$ bands of solvent water are also changed after photoisomerization. The bands of GS at 3591, 3515, 3449 cm^{-1} have shifted to 3516, 3406 and 3501, 3456 cm^{-1} for PLI1 and PLI3, respectively (see Fig. S7). The absence of these bands in case of PLI2 is expected and confirmed by IR-spectroscopy. Further, a change of the $\rho(\text{NO}_2)$ mode of GS is observed at 606 cm^{-1} . The bands corresponding to the PLI1/2 and PLI3 are found at 646 and 624 cm^{-1} , respectively. Since the $\delta(\text{NO}_2)$ bands are strongly overlapped with the bands of oxalate ligands,

the assignment of those bands is tentative (see Table 3). Likewise, the bands below 600 cm^{-1} cannot be explicitly assigned due to the overlapping with the bands of oxalate ligands. Similar changes are observed for **Rh** and **Co** compounds and summarized in Table 3.

Finally, the light-induced CO_2 release from the oxalate parts $[\text{MOx}_3]^{3-}$ is observed for all investigated compounds indicated by the appearance of a band at 2340 cm^{-1} . In case of **Cr** and **Rh** the CO_2 release occurs after a long irradiation time (more than 200 min), whereas **Co** compound exhibits a high sensitivity towards CO_2 release – the band at 2340 cm^{-1} appears even after 2 min of light irradiation (see Fig. S8). Indeed, earlier investigation of CO_2 release in the oxalate compounds showed that $[\text{CoOx}_3]^{3+}$ is quite efficiently decomposed after irradiation compared to chromium oxalate.⁴⁸

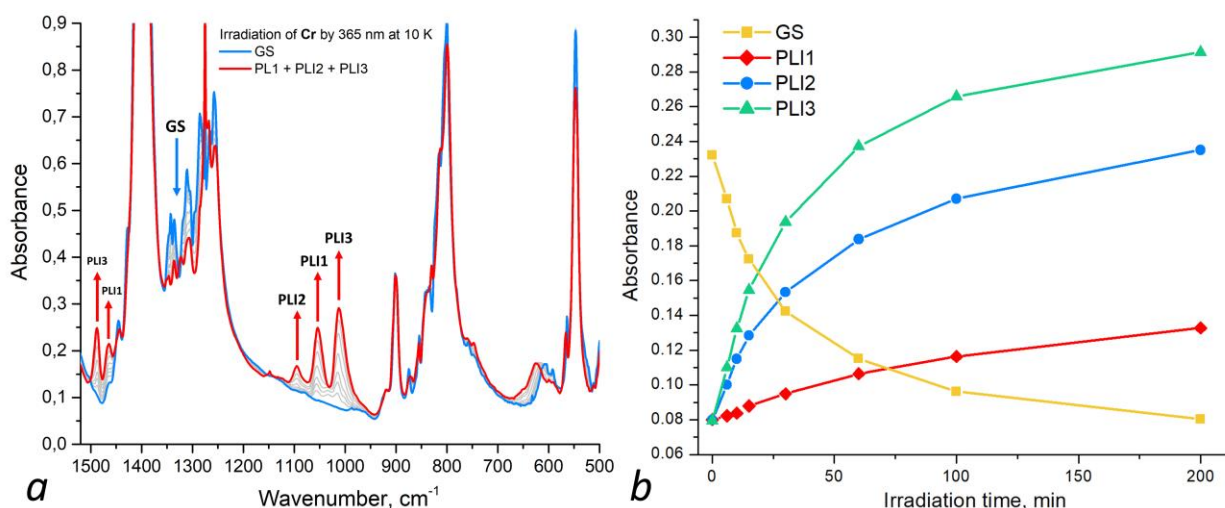


Fig. 5. Panel *a*: IR-spectra of **Cr** at 10 K before (GS) and after (PLI1 + PLI2 + PLI3) light irradiation at 365 nm; panel *b*: the evolution of intensities of the $\nu^2(\text{NO}_2)$ bands of GS and PLI1-3 during irradiation of **Cr** at 10 K with 365 nm.

Table 3. Assigned IR-bands of GS, PLI1-3 at 10 K [cm^{-1}].

Complex	Mode	GS	PLI 1	PLI2	PLI 3
Cr	$\nu(\text{OH})$	3591, 3515, 3449	3516, 3406	-	3501, 3456
	$\nu(\text{NO}_2)$	1445, 1428, 1343, 1336, 1311, 1285, 1258	1465, 1055	1442 _{sh} , 1097	1489, 1012
	$\delta(\text{NO}_2)$	824 _{sh}	835	867	830
	$\rho(\text{NO}_2)$	606	646	646	624
	Other	564, 547, 527 _{sh} , 487, 470, 420	566, 474 _{sh} , 418	-	481 _{sh}
Rh	$\nu(\text{OH})$	3594, 3519, 3454	3517, 3403	-	3502, 3457
	$\nu(\text{NO}_2)$	1454, 1425 _{sh} , 1347, 1335, 1310, 1286, 1251	1468, 1053	1444 _{sh} , 1096	1488, 1012
	$\delta(\text{NO}_2)$	822	835	867 _{sh}	830 _{sh}
	$\rho(\text{NO}_2)$	601	645	645	624
	Other	572, 555, 527 _{sh} , 478, 469, 414	561 _{sh} , 472	-	484 _{sh}
Co	$\nu(\text{OH})$	3574, 3501, 3446	3400	-	3480, 3451
	$\nu(\text{NO}_2)$	1435, 1347, 1336, 1309, 1286, 1260	1467, 1056	1440 _{sh} , 1097	1486, 1013
	$\delta(\text{NO}_2)$	822	840	864	820
	$\rho(\text{NO}_2)$	606	650	650	628

	Other	579, 567, 551, 483, 467, 451	-	-	-
--	-------	------------------------------	---	---	---

Thermal stability of PLIs

The thermal stability of PLIs was investigated by IR-spectroscopy. The reaction constants (k) of the first order thermal decay of each PLI were measured in isothermal mode at several chosen temperatures. Further, activation energies (E_a) and frequency factors ($\lg k_0$) were determined in Arrhenius coordinates (Fig. S9). Additionally, the decay temperatures (T_d) were calculated at $k = 10^{-3} \text{ s}^{-1}$. T_d is a useful parameter to compare thermal stability of different linkage isomers.⁴⁹ The kinetic data of the thermal decay of PLI1-3 in all compounds are listed in Table 4.

Table 4. Thermal stability parameters of PLIs: activation energies (E_a), frequency factors ($\lg k_0$) and decay temperatures (T_d).

	PLI1			PLI2			PLI3		
	E_a , kJ mol ⁻¹	$\lg k_0$	T_d , K	E_a , kJ mol ⁻¹	$\lg k_0$	T_d , K	E_a , kJ mol ⁻¹	$\lg k_0$	T_d , K
Cr	47.1±2.0	7.4±0.4	237±10	66.1±3.2	11.2±0.7	243±12	13.4±0.5	4.6±0.3	92±3
Rh	55.6±7.2	9.2±1.6	238±30	62.7±14.1	10.4±3.0	245±55	18.3±2.8	7.4±1.5	92±14
Co	60.9±11.4	10.3±2.4	239±45	85.2±14.4	15.5±3.1	241±41	21.1±0.4	8.9±0.2	93±2

In order to investigate thermal decay of PLI1-3, on the first stage PLIs were photogenerated at 150 or 10 K, on the second stage the decay was measured at different temperatures in isothermal conditions. The decay of PLI3 in **Cr** at 100 K is shown in Fig. 6. From Fig. 6, one can observe that PLI3 thermally decays selectively to PLI1: the bands of PLI3 at 1489 and 1012 cm⁻¹ decrease and the bands of PLI1 at 1467 and 1053 cm⁻¹ grow. Since the bands of PLI2 and GS do not change their amplitudes this indicates that a single process PLI3→PLI1 occurs. The reason why the *exo*-isomer PLI3 decays only to the *endo*-isomer PLI1, but not to the *endo*-isomer PLI2, is that PLI3 and PLI1 are related to the same crystallographic site where the nearby solvate site is occupied by a water molecule (see SCXRD section). Similar decay of the *exo*-ONO isomer to the *endo*-ONO was reported recently for a nickel complex.³⁹ As can be noted from Table 4, for different compounds the parameters E_a and $\lg k_0$ are different, however the parameter T_d is the same within error (92-93 K). We suggest that T_d is a more reliable parameter describing thermal decay by a single value, whereas E_a and $\lg k_0$ are different for each compound due to the mathematical correlation between E_a and $\lg k_0$. It seems thus that for the present case small differences in the intermolecular interactions of *exo*-ONO ligand do not affect thermal stability of PLI3.

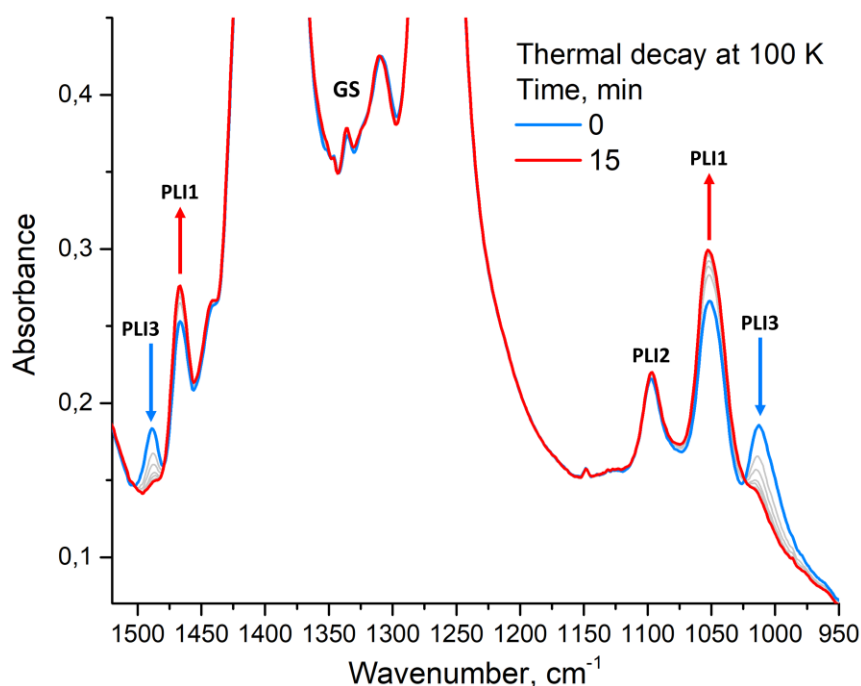


Fig. 6. The thermal evolution of IR-spectra of Cr at 100 K after photogeneration of PLIs at 10 K.

Further heating leads to an efficient decay of PLI1 and PLI2 at temperatures around 240 K (see Fig. 7). Similar to PLI3, kinetic parameters of the decay were measured and shown in Table 4. The decay temperature of PLI1 is slightly lower compared to T_d of PLI2. The difference is small but significant, indicating a higher stability for the PLI2 configuration of the *endo*-isomer, i.e. the one without neighboring water molecule. From the structural point of view, there is a difference in the intermolecular contacts of the *endo*-ONO in PLI1 and PLI2. Considering all the compounds, the average distance of the closest contact O1A-NH₃ in PLI1 is 2.88 Å, whereas the closest contact O2B-NH₃ in PLI2 is longer and reaches 3.44 Å. In addition, in the case of PLI1 the presence of the nearby water molecule results in a hydrogen bond of 2.8 Å (O2A-O3) between NO₂ and H₂O, only slightly longer than the one for GS (2.7 Å) (Fig.2). Thus, it seems that despite the stronger intermolecular interactions present in PLI1, its activation energy is slightly lower than one in PLI2. Overall, based on the thermal behavior of PLI1-3, the thermal decay process of the *exo*-ONO isomer in the investigated compounds can be schematically described as *exo*-ONO → *endo*-ONO → NO₂.

According to the theoretical¹³⁻¹⁵ and experimental²² investigations of related nitro-compounds, *exo*-isomers tend to exhibit a lower thermal stability compared to *endo*-ONO. For example, in [Pd(Et₄dien)(NO₂)]OTf complex (Et₄dien = N,N,N',N'- tetraethyldiethylene-triamine, OTf = trifluoromethanesulfonate) the *endo*-ONO isomer decays at a temperature of about 190 K, whereas the *exo*-ONO form relaxes at 120 K.²² Several theoretical works on octahedral nickel and cobalt compounds show that the nitro isomer (GS) is thermodynamically more stable and possesses lower electronic energy with respect to *endo*- and *exo*-nitrito isomers.¹³⁻¹⁵ Regarding the activation energies of the decay processes of nitrito isomers, theoretical investigations suggest that the activation barrier of *endo*-ONO → NO₂ reaction is 2-4 times higher than one for *exo*-ONO → *endo*-ONO reaction. The results obtained in the current investigation are in agreement with these theoretical conclusions made for octahedral compounds, thus, apparently, square planar nitro-nitrito compounds might exhibit similar patterns of PLI behavior.

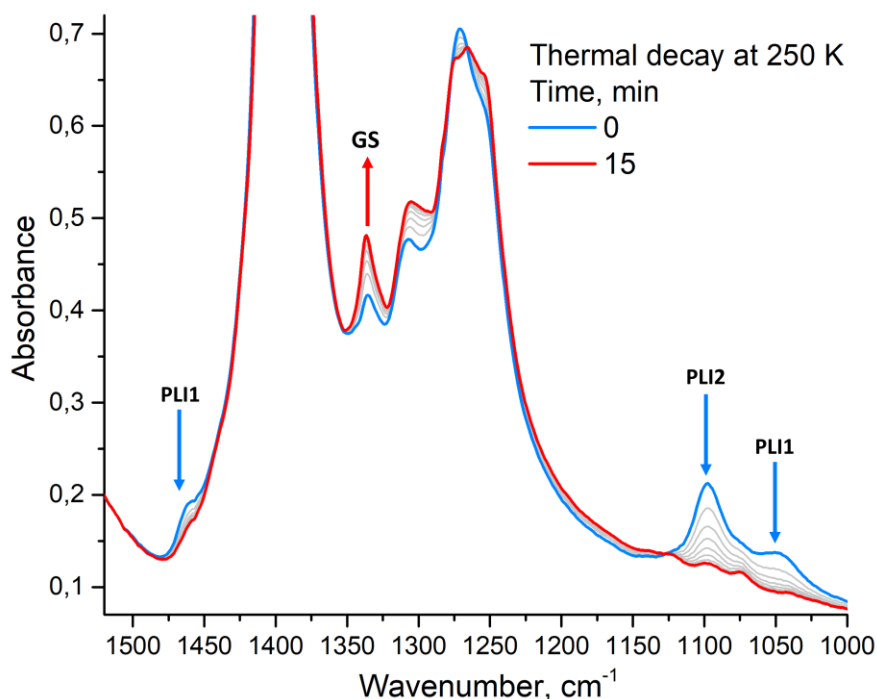


Fig. 7. The thermal evolution of IR-spectra of Cr at 250 K after photogeneration of PLIs at 150 K.

Mechanistic aspects of PLIs photogeneration

A gradual irradiation of the compounds at 10 K induces a simultaneous formation of all isomers PLI1-3 (see Fig. 5), where the efficiency of the formation and population of PLI1, 3 is higher with respect to PLI2. This observation may give us the impression that each PLI could be generated directly from GS. However, the generation of PLI3 from the mixture of GS, PLI1 and PLI2 warns from drawing such a general conclusion. In the Fig. 8 the evolution of the spectra at 50 K (where PLI1 and PLI2 were previously photogenerated at 150 K) after 365 nm irradiation is shown. The irradiation of the mixture of GS, PLI1 and PLI2 at a temperature where PLI3 is stable (50 K) leads to a depletion of the intensities of PLI1, 2 and the appearance of the bands of PLI3, whereas the bands of GS only slightly increase the amplitudes.

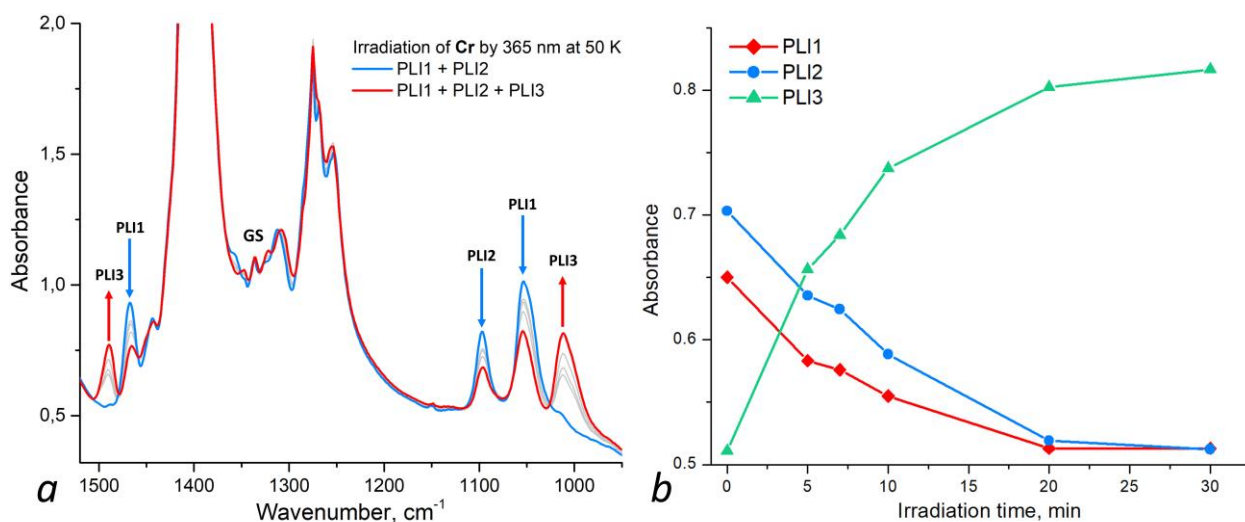


Fig. 8. Panel *a*: IR-spectra of Cr at 50 K: on the first stage PLI1 and PLI2 were generated at 150 K until the saturation (PLI1 + PLI2), on the second stage the sample was cooled down to 50 K and further irradiated at 365

nm (PLI1 + PLI2 + PLI3); panel *b*: the evolution of intensities of the $\nu^s(\text{NO}_2)$ bands of PLI1-3 during subsequent irradiation of Cr at 50 K at 365 nm.

Thus, there is a route of the photoinduced formation of PLI3 (and apparently PLI4) from PLI1 and PLI2. It is important to mention, that PLI1 and PLI3 are related to the same site with H_2O molecule. It is also possible that PLI4 has the same IR signature as PLI3, i.e. a band at 1012 cm^{-1} , which would explain naturally the transfer from PLI2 to this band. Otherwise, which is unlikely, the potential process $\text{PLI2} \rightarrow \text{PLI3}$ is expected to include several stages through the formation of GS. The situation is simpler for the $\text{PLI1} \rightarrow \text{PLI3}$ reaction, and we focus the further discussion on this case. Actually, the obtained results do not allow to exclude the $\text{GS} \rightarrow \text{PLI3}$ process, however they suggest that the photoreaction $\text{PLI1} \rightarrow \text{PLI3}$ is favorable.

Summarizing the obtained experimental results we can draw two possible mechanisms for the photoisomerization of the NO_2 ligand in the investigated system (see Fig. 9).

Scenario a:

This pathway shown in Fig. 9, panel *a*, implies photoinduced two-step process with *endo*-ONO isomer as an intermediate state towards *exo*-ONO ($\text{NO}_2 \rightarrow \text{endo-ONO} \rightarrow \text{exo-ONO}$). Thus, on the first step the light excitation of GS leads to the formation of *endo*-ONO, the following light absorption by *endo*-ONO leads the system to *exo*-ONO state. Knowing that the thermal stability of *endo*-PLI1 is much higher than that of *exo*-PLI3, the *endo*-PLI1 is stabilized at temperature below 200 K after being generated directly from GS. At these temperatures any potential population of *exo*-PLI3 immediately relaxes back to the *endo*-PLI1 due to the comparatively small activation barrier between PLI3 and PLI1. Below temperatures of 90 K the second step *endo*-PLI1 \rightarrow *exo*-PLI3 can lead to a stable population of the *exo*-isomer PLI3, as now the activation barrier is high enough preventing thermal relaxation. In this low-temperature situation, the photostationary equilibrium defining the relative populations of GS, PLI1 and PLI3 only depends on the forward and backward rates of the optical excitation. Note that this scheme does not consider or exclude the formation of other possible transient or metastable states. From the theoretical point of view, the photochemical route $\text{NO}_2 \rightarrow \text{endo-ONO} \rightarrow \text{exo-ONO}$ is also favorable.¹³⁻¹⁵ According to the calculations, the light irradiation of a NO_2 compound in GS excites the system to a transient singlet or triplet state followed by the relaxation to *endo*-ONO. The lowest LUMO orbitals of GS usually include a large contribution from antibonding orbitals of the M- NO_2 unit. As soon as the *endo*-ONO has appeared it can be excited to another transient state with further relaxation to *exo*-ONO. Importantly, the possibility of the formation of *endo*- or *exo*-isomer is also controlled by the free space required for the rotation of the NO_2 ligand, and by the activation energies of the *exo*-ONO \rightarrow *endo*-ONO and *endo*-ONO \rightarrow NO_2 reactions, which set the kinetic control of the thermal decay of PLIs at certain temperatures. However, one must be aware that above mentioned calculations have been done for octahedral systems, and for square planar species the mechanism might be different. It is important to mention that an evaluation of the mechanism of NO_2 ligand isomerization has been made for a model square planar complex $[\text{Ni}(\text{dmpe})\text{Cl}(\text{NO}_2)]$ ($\text{dmpe} = (\text{CH}_3)_2\text{PCH}_2\text{CH}_2\text{P}(\text{CH}_3)_2$).¹⁶ According to DFT calculations, the excited transient state resembles *exo*-ONO configuration having tetrahedral arrangement, however, no similar square planar *exo*-ONO linkage isomer has been found on the ground state potential energy surface.

Scenario b:

Based on the obtained experimental results another mechanism can be proposed, as schematically shown in Fig. 9, panel *b*. In this case the *exo*-ONO is considered as an intermediate state towards the formation of *endo*-ONO. Thus, the light excitation of GS drives the system to the formation of *exo*-PLI3. Due to the low activation barrier between *exo*-PLI3 and *endo*-PLI1 ($E_a \approx 0.2\text{ eV}$), at higher temperature (150 K) *exo*-PLI3 decays directly to *endo*-PLI1, while at low temperature (10 K) *exo*-PLI3 can be thermally stabilized. At this low temperature the further transformation to *endo*-PLI1 occurs thus through light excitation. As in the previous scenario, the relative

populations of the three states GS, *endo*-PLI1, and *exo*-PLI3 then depends on the optical forward and backward rates between the three states.

Finally, based on our reported experimental data and theoretical investigations performed for related octahedral systems the scenario *a* looks more favorable. However, the two scenarios presented based on our experimental results take into account only the metastable configurations on the ground state potential energy surface. In order to unravel the complicated mechanism of isomerization in this system either time resolved experiments that allow capturing a transient species or extensive DFT/TDDFT calculations are necessary.

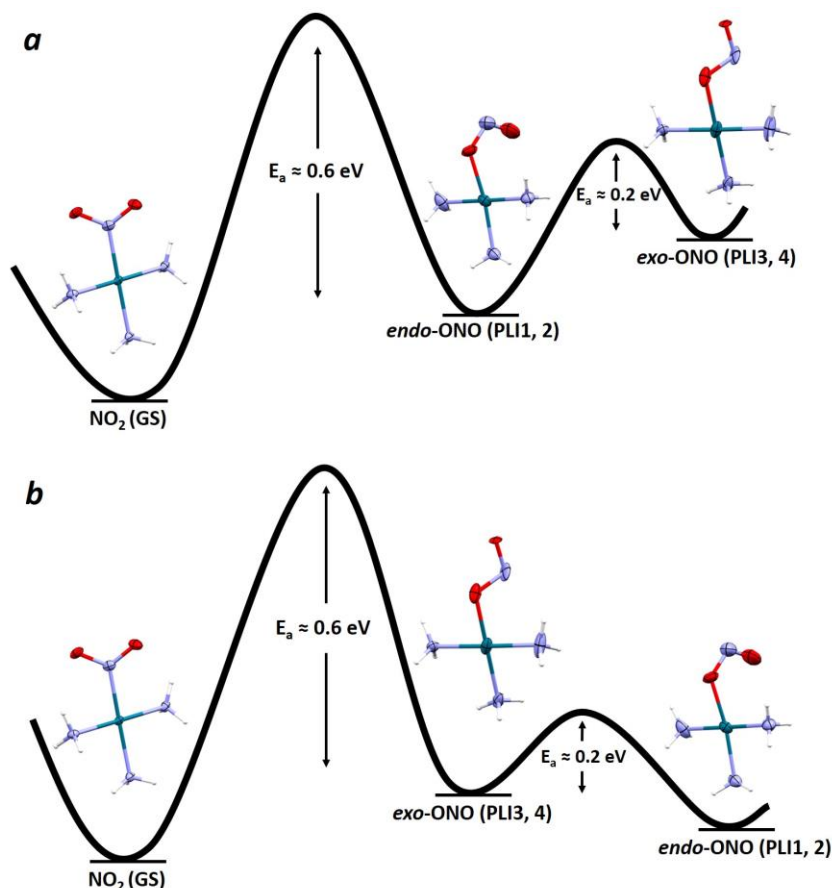


Fig. 9. Possible energetic diagrams of NO_2 ligand isomerization: panel *a* represents scenario with *endo*-ONO isomer as an intermediate state, panel *b* – the route with intermediate *exo*-ONO.

UV-vis-spectroscopy of PLIs

In order to obtain the information on the absorption properties of linkage isomers UV-vis spectra of the compounds in solution and solid state were collected. The spectra of water solutions of **Cr**, **Rh**, **Co**, corresponding oxalate salts $[\text{MOx}_3]^{3-}$ and $[\text{Pd}(\text{NH}_3)_4](\text{NO}_3)_2$ are shown in Fig. S10. In **Cr**, **Rh**, **Co** the intense bands with maxima at 420 and 570; 400; 420 and 600, respectively, are assigned to the transitions of $[\text{MOx}_3]^{3-}$ parts. The spectrum of $[\text{Pd}(\text{NH}_3)_4]^{2+}$ exhibits absorption from the UV-range up to 450 nm. Since the experimentally measured UV-vis-spectrum of $[\text{Pd}(\text{NH}_3)_3(\text{NO}_2)]^+$ is unknown, and the isomerization reactions are accessible only by 365-405 nm light, we can only state that $[\text{Pd}(\text{NH}_3)_3(\text{NO}_2)]^+$ absorbs in this region, and that it corresponds most probably to a band involving NO_2 orbital contributions. Concerning the difference in PLIs conversion for the different compounds, a possible reason of the lower population of PLIs in **Rh** is the relatively strong absorption of $[\text{RhOx}_3]^{3-}$ anion making the excitation of $[\text{Pd}(\text{NH}_3)_3(\text{NO}_2)]^+$ less probable (see Fig. S10).

The solid state UV-vis-spectrum of **Cr** in KBr matrix at 150 K is shown in Fig. 10, *a*. The spectrum shows bands similar to those in the spectrum of water solution. Photogeneration of PLI1, 2 leads to an increase of absorption

in the UV-range (280-450 nm, Fig. 9, *a*, insert), which supports proposed mechanisms of photoinduced reaction *endo*-ONO→*exo*-ONO, since the bands potentially allowing the reaction exist at the excitation wavelength. The difference spectrum of PLI3 measured at 10 K exhibit similar features and are shown in Fig. 10, *b*, permitting photoinduced transfer *exo*-ONO→*endo*-ONO.

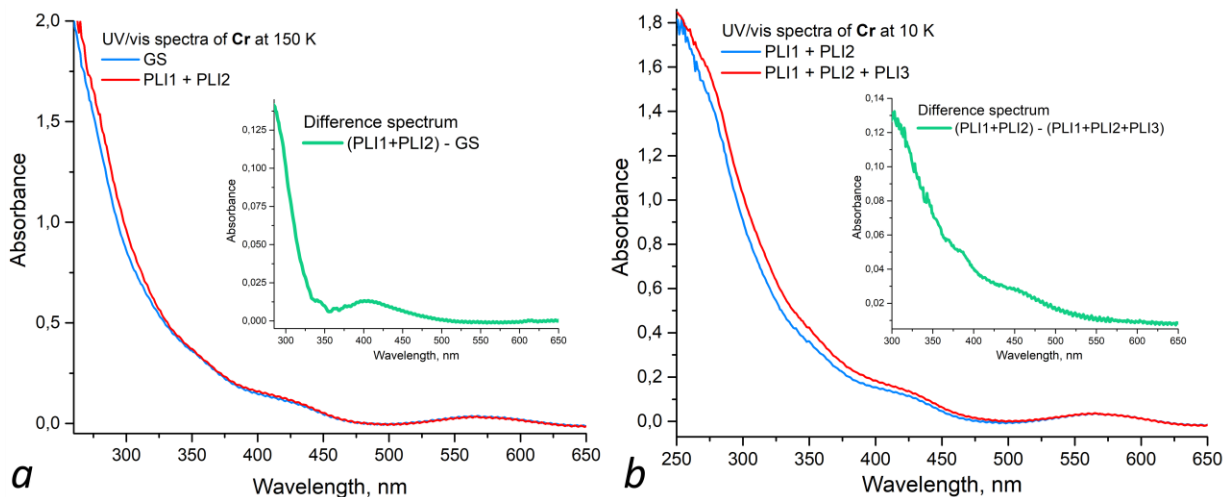


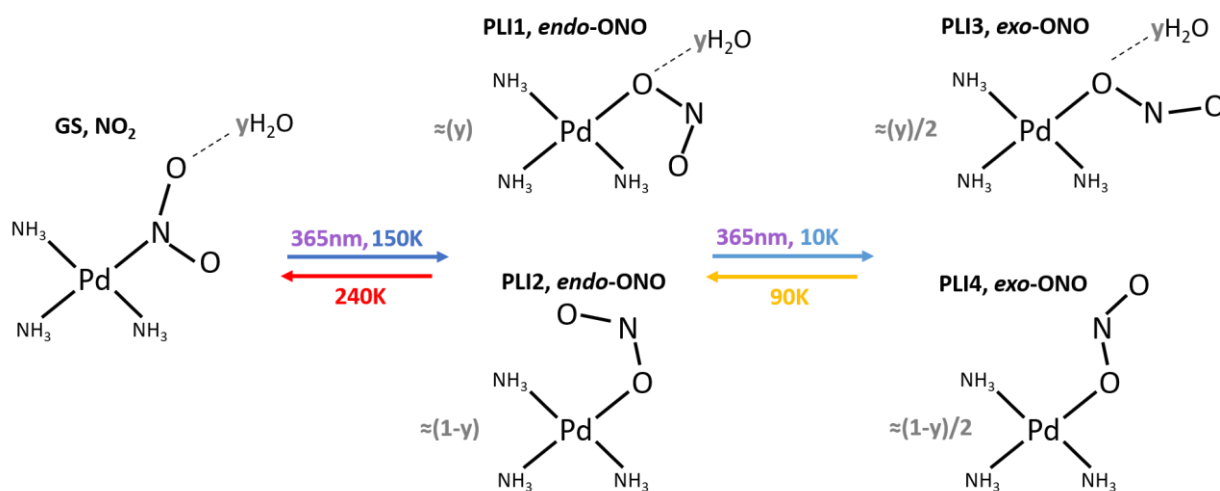
Fig. 10. UV-vis-spectra of Cr in KBr pellets: *a*) spectra of GS and PLI1, 2 at 150 K and corresponding difference spectrum in the insert; *b*) spectra of PLI1, 2 and PLI1-3 at 10 K and corresponding difference spectrum in the insert. Similar to Fig. 8, on the first stage (*a*) PLI1 and PLI2 were generated at 150 K until the saturation (PLI1 + PLI2), on the second stage (*b*) the sample was cooled down to 10 K and further irradiated by 365 nm (PLI1 + PLI2 + PLI3).

Conclusions

The properties of photoinduced linkage isomers (PLIs) in a square planar complex $[\text{Pd}(\text{NH}_3)_3\text{NO}_2]^+$ being a part of the complex salts $[\text{Pd}(\text{NH}_3)_4][\text{Pd}(\text{NH}_3)_3\text{NO}_2][\text{MOx}_3] \cdot y\text{H}_2\text{O}$ ($\text{M} = \text{Cr}$ (**Cr**), Rh (**Rh**), Co (**Co**), $\text{Ox} = \text{oxalate}$) were investigated. It was shown by XRD, that the irradiation at 365 nm at 150 K of the single crystals of **Cr**, **Rh** and **Co** leads to the formation of *endo*-ONO isomers PLI1 and PLI2. PLI1 and PLI2 differ in their intermolecular surrounding, where the partial occupation of a neighboring site by a solvate water molecule prevents the photoinduced formation of PLI2. Considering the fact that the water content could be adjusted, the structural tuning of the linkage isomers is possible in these systems. The total population of *endo*-ONO isomers in **Cr**, **Co** and **Rh** is 83, 40 and 29%, respectively. Further, on the example of **Cr** compound, PLIs were photogenerated at 10 K. Photocrystallographic analysis reveals the formation of *exo*-ONO isomers PLI3 and PLI4, which are not sufficiently stable at 80 K. Thus, four different PLIs can be photogenerated in $[\text{Pd}(\text{NH}_3)_3\text{NO}_2]^+$, moreover, the type and population of PLIs could be influenced by the amount of solvent H_2O molecules, by the type of $[\text{MOx}_3]^{3-}$ and by the temperature of the photogeneration.

Given the knowledge on the structures of PLI1-4 revealed by photocrystallography, the population/depopulation dynamics of PLIs was investigated in more detail using IR-spectroscopy in the temperature range of 10-300 K. As soon as a PLI appears its stability is governed by the kinetic parameters E_a and $\lg k_0$. A gradual heating of the PLIs showed that *endo*-ONO and *exo*-ONO isomers in the complexes have a different thermal stability and different decay paths. Namely, the *exo*-ONO isomer decays to the *endo*-ONO, further heating of the *endo*-ONO leads to its decay to the GS nitro isomer NO_2 . Thus, the thermal decay of *exo*-ONO and *endo*-ONO isomers occurs via the scheme *exo*-ONO→*endo*-ONO→ NO_2 (see Scheme 1). On the example of *endo*-ONO isomers PLI1 and PLI2, a small difference in the thermal stability of *endo*-ONO could be

related to a different strength of the intermolecular interactions of *endo*-ONO or NO₂ isomers, however, no specific parameters affecting the stability have yet been found. The investigation of the forward photoinduced reaction revealed presumable routes of PLIs generation. Accordingly, the mechanism of the photogeneration of *exo*-ONO rather can be described as NO₂→*endo*-ONO→*exo*-ONO process, thus likely two photons are needed to generate *exo*-ONO from GS. However, to prove the mechanism and to rule out the NO₂→*exo*-ONO→*endo*-ONO scenario further investigations are needed. It is important to emphasize, that both forward and backward processes are strongly affected by the nearest surrounding of the photoswitchable ligand, since the parameters such as reaction cavity shape and volume can influence the thermal stability and a possibility of the generation of a certain PLI. The presented results show that the complex [Pd(NH₃)₃NO₂]⁺ can be used as a convenient and simple model compound for the theoretical investigation of the nitro-nitrito isomerization in square planar species.



Scheme 1. The photo- and thermally induced transformations in $\text{Cr}([\text{Pd}(\text{NH}_3)_4][\text{Pd}(\text{NH}_3)_3\text{NO}_2][\text{MOx}_3]\cdot y\text{H}_2\text{O})$, $\text{M} = \text{Cr}$ (**Cr**), Rh (**Rh**), Co (**Co**), $\text{Ox} = \text{oxalate}$). The coefficients roughly represent the populations of the linkage isomers, the populations of PLIs in case of **Rh** and **Co** are lower.

Acknowledgements

The work has been supported by grant of ANR (grant no. ANR-21-CE30-0045-01). Artem Mikhailov is grateful for financial support from the Metchnikov bourse program 2021. We thank the PMD2X platform of Université de Lorraine for granting access to XRD diffractometers.

ASSOCIATED CONTENT

Supporting Information available. IS contains crystallographic and structural data (Table S1, S2; Fig. S1, S2); additional IR and UV-vis spectroscopy data (Fig. S3-S10).

References

- (1) Browne, W. R.; Feringa, B. L. Chiroptical Molecular Switches. *Mol. Switch. Second Ed.* **2011**, *1*, 121–179. <https://doi.org/10.1002/9783527634408.ch5>.
- (2) Feringa, B. L. The Art of Building Small: From Molecular Switches to Motors (Nobel Lecture). *Angew. Chemie Int. Ed.* **2017**, *56* (37), 11060–11078. <https://doi.org/10.1002/anie.201702979>.

- (3) Hatcher, L. E.; Skelton, J. M.; Warren, M. R.; Raithby, P. R. Photocrystallographic Studies on Transition Metal Nitrito Metastable Linkage Isomers: Manipulating the Metastable State. *Acc. Chem. Res.* **2019**, *52* (4), 1079–1088. <https://doi.org/10.1021/acs.accounts.9b00018>.
- (4) Hatcher, L. E.; Warren, M. R.; Allan, D. R.; Brayshaw, S. K.; Johnson, A. L.; Fuertes, S.; Schiffers, S.; Stevenson, A. J.; Teat, S. J.; Woodall, C. H.; Raithby, P. R. Metastable Linkage Isomerism in [Ni(Et₄dien)(NO₂)₂]: A Combined Thermal and Photocrystallographic Structural Investigation of a Nitro/Nitrito Interconversion. *Angew. Chemie - Int. Ed.* **2011**, *50* (36), 8371–8374. <https://doi.org/10.1002/anie.201102022>.
- (5) Hatcher, L. E.; Christensen, J.; Hamilton, M. L.; Trincão, J.; Allan, D. R.; Warren, M. R.; Clarke, I. P.; Towrie, M.; Fuertes, D. S.; Wilson, C. C.; Woodall, C. H.; Raithby, P. R. Steady-State and Pseudo-Steady-State Photocrystallographic Studies on Linkage Isomers of [Ni(Et₄Dien)(η²-O,ON)(η¹-NO₂)]: Identification of a New Linkage Isomer. *Chem. – A Eur. J.* **2014**, *20* (11), 3128–3134. <https://doi.org/10.1002/chem.201304172>.
- (6) Ahmed, E.; Chizhik, S.; Sidel'nikov, A.; Boldyreva, E.; Naumov, P. Relating Excited States to the Dynamics of Macroscopic Strain in Photoresponsive Crystals. *Inorg. Chem.* **2022**, *61* (8), 3573–3585. <https://doi.org/10.1021/acs.inorgchem.1c03607>.
- (7) Schaniel, D.; Bendeif, E.-E.; Woike, T.; Böttcher, H.-C.; Pillet, S. Wavelength-Selective Photoisomerisation of Nitric Oxide and Nitrite in a Rhodium Complex. *CrystEngComm* **2018**, *20* (44), 7100–7108. <https://doi.org/10.1039/C8CE01345D>.
- (8) Borowski, P.; Kutniewska, S. E.; Kamiński, R.; Krówczyński, A.; Schaniel, D.; Jarzemska, K. N. Exploring Photoswitchable Properties of Two Nitro Nickel(II) Complexes with (N, N, O)-Donor Ligands and Their Copper(II) Analogues. *Inorg. Chem.* **2022**, *61* (17), 6624–6640. <https://doi.org/10.1021/acs.inorgchem.2c00526>.
- (9) Warren, M. R.; Brayshaw, S. K.; Hatcher, L. E.; Johnson, A. L.; Schiffers, S.; Warren, A. J.; Teat, S. J.; Warren, J. E.; Woodall, C. H.; Raithby, P. R. Photoactivated Linkage Isomerism in Single Crystals of Nickel, Palladium and Platinum Di-Nitro Complexes – a Photocrystallographic Investigation. *Dalt. Trans.* **2012**, *41* (42), 13173. <https://doi.org/10.1039/c2dt30314k>.
- (10) Chizhik, S.; Sidel'nikov, A.; Zakharov, B.; Naumov, P.; Boldyreva, E. Quantification of Photoinduced Bending of Dynamic Molecular Crystals: From Macroscopic Strain to Kinetic Constants and Activation Energies. *Chem. Sci.* **2018**, *9* (8), 2319–2335. <https://doi.org/10.1039/C7SC04863G>.
- (11) Deresz, K. A.; Kamiński, R.; Kutniewska, S. E.; Krówczyński, A.; Schaniel, D.; Jarzemska, K. N. An Optically Reversible Room-Temperature Solid-State Cobalt(III) Photoswitch Based on Nitro-to-Nitrito Linkage Isomerism. *Chem. Commun.* **2022**, *58* (97), 13439–13442. <https://doi.org/10.1039/D2CC05134F>.
- (12) Schaniel, D.; Mockus, N.; Woike, T.; Klein, A.; Sheptyakov, D.; Todorova, T.; Delley, B. Reversible Photoswitching between Nitrito-N and Nitrito-O Isomers in Trans-[Ru(Py)₄(NO₂)₂]. *Phys. Chem. Chem. Phys.* **2010**, *12* (23), 6171. <https://doi.org/10.1039/b921723a>.
- (13) Skelton, J. M.; Crespo-Otero, R.; Hatcher, L. E.; Parker, S. C.; Raithby, P. R.; Walsh, A. Energetics, Thermal Isomerisation and Photochemistry of the Linkage-Isomer System [Ni(Et₄Dien)(η²-O,ON)(η¹-NO₂)]. *CrystEngComm* **2015**, *17* (2), 383–394. <https://doi.org/10.1039/C4CE01411A>.
- (14) Muya, J. T.; Chung, H.; Lee, S. U. Theoretical Investigation on the Ground State Properties of the Hexaamminecobalt(III) and Nitro–Nitrito Linkage Isomerism in Pentaamminecobalt(III) *in Vacuo*. *RSC Adv.* **2018**, *8* (6), 3328–3342. <https://doi.org/10.1039/C7RA11603A>.
- (15) Muya, J. T.; Meher, B. R.; Sahoo, S. C.; Chung, H. A Theoretical Insight into the Role of Counter Anions and Their Interactions in Nitropentaamminecobalt(III) toward Linkage Isomerism-induced Photochemical Motion. *Int. J. Quantum Chem.* **2019**, *119* (14), e25929.

<https://doi.org/10.1002/qua.25929>.

- (16) Warren, M. R.; Easun, T. L.; Brayshaw, S. K.; Deeth, R. J.; George, M. W.; Johnson, A. L.; Schiffrs, S.; Teat, S. J.; Warren, A. J.; Warren, J. E.; Wilson, C. C.; Woodall, C. H.; Raithby, P. R. Solid-State Interconversions: Unique 100% Reversible Transformations between the Ground and Metastable States in Single-Crystals of a Series of Nickel(II) Nitro Complexes. *Chem. – A Eur. J.* **2014**, *20* (18), 5468–5477. <https://doi.org/10.1002/chem.201302053>.
- (17) Kutniewska, S. E.; Krówczyński, A.; Kamiński, R.; Jarze mbska, K. N.; Pillet, S.; Wenger, E.; Schaniel, D. Photocrystallographic and Spectroscopic Studies of a Model (N,N,O)-Donor Square-Planar Nickel(II) Nitro Complex: In Search of High-Conversion and Stable Photoswitchable Materials. *IUCrJ* **2020**, *7* (6), 1188–1198. <https://doi.org/10.1107/S205225252001307X/LQ5032SUP15.PDF>.
- (18) Sabbani, S.; Das, S. K. Reversible Nitro–Nitrito Inter-Conversion in a Simple Mono-Nuclear Nickel(II) Complex $[\text{Ni}(\text{C}_6\text{H}_4(\text{NH}_2)_2)_2(\text{NO}_2)_2]$ in the Solid State. *Inorg. Chem. Commun.* **2009**, *12* (5), 364–367. <https://doi.org/10.1016/j.inoche.2009.02.011>.
- (19) Chao, M.-S.; Lu, H.-H.; Tsai, M.-L.; Lin, C.-M.; Wu, M.-P. Thermochromic Nitro–Nitrito Interconversion Mediated by Weak-Linked Amide in Nickel (II) Diaminodiamide Complexes in the Solid State. *Inorg. Chem. Commun.* **2012**, *24* (2), 254–258. <https://doi.org/10.1016/j.inoche.2012.07.001>.
- (20) Nakamura, I.; Funasako, Y.; Mochida, T. Nitro–Nitrito Photoisomerization of Platinum(II) Complexes with $\text{Pt}(\text{NO}_2)_4^{2-}$ and $(\text{FSO}_2)_2\text{N}^-$ Anions: Correlation between Isomerization Ratio and Reaction Cavity. *Cryst. Growth Des.* **2020**, *20* (12), 8047–8052. <https://doi.org/10.1021/acs.cgd.0c01294>.
- (21) Nakamura, I.; Sumitani, R.; Mochida, T. Nitro–Nitrito Photoisomerization of Cationic Platinum(II) Complexes in the Solid State: Reactivity in Polymorphic Crystals and Glassy State. *Cryst. Growth Des.* **2021**, *21* (3), 1861–1868. <https://doi.org/10.1021/acs.cgd.1c00004>.
- (22) Hatcher, L. E.; Raithby, P. R. The Impact of Hydrogen Bonding on 100% Photo-Switching in Solid-State Nitro–Nitrito Linkage Isomers. *CrystEngComm* **2017**, *19* (42), 6297–6304. <https://doi.org/10.1039/C7CE01366C>.
- (23) Jörgensen, S. M. Zur Konstitution Der Kobalt-, Chrom- Und Rhodiumbasen. V. *Zeitschrift für Anorg. Chemie* **1894**, *5* (1), 147–196. <https://doi.org/10.1002/zaac.18940050119>.
- (24) Heyns, A. M.; de Waal, D. An Infrared Study of the Nitro–Nitrito Linkage Isomerization in Solid Nitro- and Nitritopentamminecobalt(III) Chloride. *Spectrochim. Acta Part A Mol. Spectrosc.* **1989**, *45* (9), 905–909. [https://doi.org/10.1016/0584-8539\(89\)80146-1](https://doi.org/10.1016/0584-8539(89)80146-1).
- (25) Boldyreva, E. V. Intramolecular Linkage Isomerization in the Crystals of Some Co(III) - Ammine Complexes - A Link Between Inorganic and Organic Solid State Chemistry. *Mol. Cryst. Liq. Cryst. Sci. Technol. Sect. A. Mol. Cryst. Liq. Cryst.* **1994**, *242* (1), 17–52. <https://doi.org/10.1080/10587259408037736>.
- (26) Boldyreva, E. V.; Burleva, L. P.; Burgina, E. B.; Baltachinov, V. P.; Ahsbahs, H.; Uchtmann, H.; Douleпов, V. E. Effect of High Pressure on the Infrared Spectra of Solid Nitro- and Nitrito-Cobalt(III) Ammine Complexes. *Berichte der Bunsengesellschaft für Phys. Chemie* **1992**, *96* (7), 931–937. <https://doi.org/10.1002/bbpc.19920960714>.
- (27) Naumov, P.; Sahoo, S. C.; Zakharov, B. A.; Boldyreva, E. V. Dynamic Single Crystals: Kinematic Analysis of Photoinduced Crystal Jumping (The Photosalient Effect). *Angew. Chemie Int. Ed.* **2013**, *52* (38), 9990–9995. <https://doi.org/10.1002/anie.201303757>.
- (28) Khranenko, S. P.; Kuratieva, N. V.; Gromilov, S. A. Crystal Structures of $[\text{Pd}(\text{NH}_3)_3(\text{NO}_2)][\text{Rh}(\text{NH}_3)_2(\text{NO}_2)_4]$ and $[\text{PdEn}_2][\text{Rh}(\text{NH}_3)(\text{NO}_2)_5] \cdot 0.75\text{H}_2\text{O}$. *J. Struct. Chem.* **2014**, *55* (3), 498–502. <https://doi.org/10.1134/S0022476614030160>.

- (29) Gladysheva, M. V.; Plyusnin, P. E.; Komarov, V. Y.; Tsygankova, A. R.; Gerasimov, E. Y.; Shubin, Y. V.; Korenev, S. V. COMPLEX SALTS [Pd(NH₃)₄][Pd(NH₃)₃NO₂] [CrO_x]₃·H₂O AND [Pd(NH₃)₄][Pd(NH₃)₃NO₂] [CoO_x]₃·H₂O AND SOLID SOLUTIONS [Pd(NH₃)₄][Pd(NH₃)₃NO₂][CoO_x]₃[RhO_x]₃1-X·H₂O : PROMISING PRECURSORS FOR POROUS NANOALLOYS. *J. Struct. Chem.* **2022**, *63* (4), 556–568. <https://doi.org/10.1134/S0022476622040060>.
- (30) Gladysheva, M. V.; Plyusnin, P. E.; Vorobyeva, S. N.; Komarov, V. Y.; Tkachev, S. V.; Shubin, Y. V.; Korenev, S. V. COMPLEX SALT [Pd(NH₃)₄][Pd(NH₃)₃NO₂][RhO_x]₃·H₂O AS A PROSPECTIVE PRECURSOR OF Pd–Rh NANOALLOYS. CRYSTAL STRUCTURE OF Na₃[RhO_x]₃·4H₂O. *J. Struct. Chem.* **2021**, *62* (5), 782–793. <https://doi.org/10.1134/S0022476621050140>.
- (31) CrysAlisPro Software System. Rigaku Corporation: Oxford 2016.
- (32) Sheldrick, G. M. SHELXT - Integrated Space-Group and Crystal-Structure Determination. *Acta Crystallogr. Sect. A Found. Crystallogr.* **2015**, *71* (1), 3–8. <https://doi.org/10.1107/S2053273314026370>.
- (33) Sheldrick, G. M. Crystal Structure Refinement with SHELXL. *Acta Crystallogr. Sect. C Struct. Chem.* **2015**, *71* (1), 3–8. <https://doi.org/10.1107/S2053229614024218>.
- (34) Dolomanov, O. V.; Bourhis, L. J.; Gildea, R. J.; Howard, J. A. K.; Puschmann, H. OLEX2: A Complete Structure Solution, Refinement and Analysis Program. *J. Appl. Crystallogr.* **2009**, *42* (2), 339–341. <https://doi.org/10.1107/S0021889808042726>.
- (35) Pillet, S. Time-Resolved Structural Analysis: Probing Condensed Matter in Motion. In *Structures on Different Time Scales*; De Gruyter, 2018; pp 143–220. <https://doi.org/10.1515/9783110433920-005>.
- (36) Macrae, C. F.; Sovago, I.; Cottrell, S. J.; Galek, P. T. A.; McCabe, P.; Pidcock, E.; Platings, M.; Shields, G. P.; Stevens, J. S.; Towler, M.; Wood, P. A. Mercury 4.0: From Visualization to Analysis, Design and Prediction. *J. Appl. Crystallogr.* <https://doi.org/10.1107/S1600576719014092>.
- (37) Hatcher, L. E.; Skelton, J. M.; Warren, M. R.; Stubbs, C.; Da Silva, E. L.; Raithby, P. R. Monitoring Photo-Induced Population Dynamics in Metastable Linkage Isomer Crystals: A Crystallographic Kinetic Study of [Pd(Bu₄Dien)NO₂]BPh₄. *Phys. Chem. Chem. Phys.* **2018**, *20* (8), 5874–5886. <https://doi.org/10.1039/C7CP05422J>.
- (38) Spek, A. L. Structure Validation in Chemical Crystallography. *Acta Crystallogr. Sect. D Biol. Crystallogr.* **2009**, *65* (2), 148–155. <https://doi.org/10.1107/S090744490804362X>.
- (39) Kutniewska, S. E.; Kamiński, R.; Buchowicz, W.; Jarzembska, K. N. Photo- A Nd Thermoswitchable Half-Sandwich Nickel(II) Complex: [Ni(H₅-C₅H₅)(IMes)(H₁-NO₂)]. *Inorg. Chem.* **2019**, *58* (24), 16712–16721. https://doi.org/10.1021/ACS.INORGCHEM.9B02836/SUPPL_FILE/IC9B02836_SI_001.PDF.
- (40) Zimmerman, H. E.; Nesterov, E. E. Quantitative Cavities and Reactivity in Stages of Crystal Lattices: Mechanistic and Exploratory Organic Photochemistry. *J. Am. Chem. Soc.* **2002**, *124* (11), 2818–2830. https://doi.org/10.1021/JA0124562/SUPPL_FILE/JA0124562_S.PDF.
- (41) Zimmerman, H. E.; Nesterov, E. E. Development of Experimental and Theoretical Crystal Lattice Organic Photochemistry: The Quantitative Cavity. Mechanistic and Exploratory Organic Photochemistry1. *Acc. Chem. Res.* **2002**, *35* (2), 77–85. <https://doi.org/10.1021/AR000210G>.
- (42) Konieczny, K. A.; Szczurek, A.; Bąkowiec, J.; Siedlecka, R.; Ciesielski, A.; Cyrański, M. K.; Turowska-Tyrk, I. The Reasons for Different Kinetics of the Norrish-Yang Reaction in Crystals. Structural and Spectroscopic Studies. *Cryst. Growth Des.* **2020**, *20* (8), 5061–5071. https://doi.org/10.1021/ACS.CGD.0C00245/ASSET/IMAGES/LARGE/CG0C00245_0005.JPEG.

- (43) Konieczny, K. A.; Bakowicz, J.; Paliwoda, D.; Warren, M. R.; Ciesielski, A.; Cyranski, M. K.; Turowska-Tyrk, I. Structural Reasons for the Formation of Multicomponent Products and the Influence of High Pressure. *Acta Crystallogr. Sect. B Struct. Sci. Cryst. Eng. Mater.* **2021**, *77* (3), 307–308. <https://doi.org/10.1107/S2052520621004492/FULL>.
- (44) Li, R.; Crystengcomm, /; Hatcher, L. E. Understanding Solid-State Photoswitching in [Re(OMe 2-Bpy)(CO) 3(η 1 -NO 2)] Crystals via in Situ Photocrystallography. *CrystEngComm* **2018**, *20* (39), 5990–5997. <https://doi.org/10.1039/C8CE00774H>.
- (45) Coulson, B. A.; Hatcher, L. E. Exploring the Influence of Polymorphism and Chromophore Co-Ligands on Linkage Isomer Photoswitching in [Pd(IJbpy4dca)IINO 2] 2] † ‡. *Cite this CrystEngComm* **2022**, *24*, 3701. <https://doi.org/10.1039/d2ce00213b>.
- (46) Brayshaw, S. K.; Easun, T. L.; George, M. W.; Griffin, A. M. E.; Johnson, A. L.; Raithby, P. R.; Savarese, T. L.; Schiffers, S.; Warren, J. E.; Warren, M. R.; Teat, S. J. Photocrystallographic Identification of Metastable Nitrito Linkage Isomers in a Series of Nickel(<sc>ii</sc>) Complexes. *Dalt. Trans.* **2012**, *41* (1), 90–97. <https://doi.org/10.1039/C1DT11379H>.
- (47) Warren, M. R.; Brayshaw, S. K.; Johnson, A. L.; Schiffers, S.; Raithby, P. R.; Easun, T. L.; George, M. W.; Warren, J. E.; Teat, S. J. Reversible 100 % Linkage Isomerization in a Single-Crystal to Single-Crystal Transformation: Photocrystallographic Identification of the Metastable [Ni(Dppe)(η 1 -ONO)Cl] Isomer. *Angew. Chemie Int. Ed.* **2009**, *48* (31), 5711–5714. <https://doi.org/10.1002/anie.200901706>.
- (48) Sugimori, A. The Radiolysis of Crystalline Oxalato Metal Complexes. The Effects of Coordinating Metal Ions on the Radiolysis of Oxalate. *Bull. Chem. Soc. Jpn.* **1966**, *39* (12), 2583–2588. <https://doi.org/10.1246/bcsj.39.2583>.
- (49) Morioka, Y.; Ishikawa, A.; Tomizawa, H.; Miki, E. Light-Induced Metastable States in Nitrosyl–Ruthenium Complexes Containing Ethylenediamine and Oxalate Ion Ligands. *J. Chem. Soc. Dalt. Trans.* **2000**, *54* (5), 781–786. <https://doi.org/10.1039/a906429j>.

Supplementary Material: Photogeneration of several linkage isomers and investigation of forward and backward nitro-nitrito isomerization processes in a palladium complex

Artem Mikhailov^{a*}, Krzysztof A. Konieczny^{a,b}, Maria Gladysheva^{c,d}, Pavel Plyusnin^c, Sébastien Pillet^a,
Dominik Schaniel^a

*Corresponding author: artem.mikhailov.a@gmail.com

^a Université de Lorraine, CNRS, CRM2, UMR 7036, Nancy 54000, France

^b Institute of Advanced Materials, Wrocław University of Science and Technology, Wybrzeże Wyspiańskiego 27, 50-370 Wrocław, Poland

^c Nikolaev Institute of Inorganic Chemistry, Siberian Branch of the Russian Academy of Sciences, 3 Acad. Lavrentiev Avenue, Novosibirsk 630090, Russian Federation

^d Novosibirsk State University, Pirogova 1, Novosibirsk 630090, Russian Federation

Table S1. Selected crystallographic data. For all structures: crystal system = monoclinic; space group = P2₁/n; Z, Z' = 4, 1.

Structure	Co (GS)	Co (GS+PLI1, 2)	Rh (GS)	Rh (GS+PLI1, 2)
Irradiation time, 365 nm [min]	0	60	0	240
Temperature [K]	150	150	150	150
GS population [%]	100	60.1	100	70.7
M _r	713.92	713.92	757.84	757.85
Crystal dimensions [mm]	0.357 × 0.307 × 0.127	0.357 × 0.307 × 0.127	0.461 × 0.293 × 0.219	0.461 × 0.293 × 0.219
a [Å]	8.0984(2)	8.1322(2)	8.11747(15)	8.1436(2)
b [Å]	13.0299(4)	13.1555(5)	13.1250(3)	13.1617(4)
c [Å]	19.9015(5)	19.8593(6)	20.0572(4)	20.0440(6)
β [°]	95.784(2)	96.256(3)	96.2711(19)	96.550(3)
Volume [Å ³]	2089.35(10)	2111.96(12)	2124.14(8)	2134.35(10)
D _x [g/cm ³]	2.270	2.245	2.370	2.358
μ [mm ⁻¹]	2.575	2.574	2.529	2.517
Reflections collected	54691	50030	56489	56281
Reflections independent	8504	7332	8648	8695
Reflections observed [Fo > 4σ(Fo)]	7125	5526	7610	7452
Completeness [%]	100	100	100	100
R _{int}	0.0542	0.0723	0.0534	0.0617
R [F ² >2(F ²)], wR, S	0.0280, 0.0639, 1.104	0.0562, 0.1613, 1.135	0.0256, 0.0598, 1.102	0.0572, 0.1204, 1.343
Δρ _{max} , Δρ _{min} [eÅ ⁻³]	1.111, -1.433	3.543, -2.303	1.043, -1.553	2.603, -2.321

Structure	Cr (GS)	Cr (GS+PLI1, 2)	Cr (GS)	Cr (GS+PLI1, 2, 3, 4)
Irradiation time, 365 nm [min]	0	60	0	30
Temperature [K]	150	150	10	10
GS population [%]	100	17.4	100	39.2
M _r	706.76	706.38	703.38	703.04
Crystal dimensions [mm]	0.378 × 0.263 × 0.119	0.378 × 0.263 × 0.119	0.320 × 0.180 × 0.158	0.320 × 0.180 × 0.158
a [Å]	8.1355(2)	8.2028(2)	8.1106(3)	8.1372(4)
b [Å]	13.1028(3)	13.2208(3)	13.0066(7)	13.1598(8)
c [Å]	19.9916(5)	19.8854(5)	19.9569(10)	19.9519(11)
β [°]	95.969(2)	96.748(2)	95.933(4)	96.584(5)
Volume [Å ³]	2119.50(9)	2141.58(9)	2093.99(17)	2122.43(19)

D_x [g/cm ³]	2.215	2.192	2.231	2.200
μ [mm ⁻¹]	2.268	2.245	2.278	2.278
Reflections collected	54679	54065	19498	19784
Reflections independent	8643	8388	8552	8668
Reflections observed [Fo > 4sig(Fo)]	7256	6717	7573	7220
Completeness [%]	100	100	100	100
R _{int}	0.0528	0.0612	0.0269	0.0326
R [F ² >2(F ²)], wR, S	0.0270, 0.0617, 1.100	0.0328, 0.0747, 1.217	0.0313, 0.0782, 1.027	0.0446, 0.0895, 1.166
$\Delta\rho_{\max}, \Delta\rho_{\min}$ [eÅ ⁻³]	1.186, -1.189	1.069, -1.578	1.914, -1.784	1.862, -3.021

Table S2. The hydrogen bond between water molecule and photoreactive ligand.

T, K	Structure	HB	D...A [°]	\angle DHA [°]
150	Co (GS)	O3-H3E...O2	2.727(4)	176.64(19)
	Co (GS+PLI1, 2)	O3-H3E...O2	2.720(14)	169.5(6)
		O3-H3E...O2A	2.69(3)	144.7(10)
150	Rh (GS)	O3-H3E...O2	2.754(4)	164.05(19)
	Rh (GS+PLI1, 2)	O3-H3E...O2	2.722(12)	172.1(5)
		O3-H3E...O2A	2.84(3)	155.2(12)
150	Cr (GS)	O3-H3E...O2	2.746(4)	167.35(19)
	Cr (GS+PLI1, 2)	O3-H3E...O2	2.72(3)	154.6(6)
		O3-H3E...O2A	2.750(7)	174.7(3)
10	Cr (GS)	O3-H3D...O2	2.735(4)	166.7(2)
	Cr (GS+PLI1, 2, 3, 4)	O3-H3E...O2	2.422(12)	166.0(4)
		O3-H3E...O2A	2.493(17)	156.9(8)
		O3-H3E...O2C	3.037(9)	158.0(4)

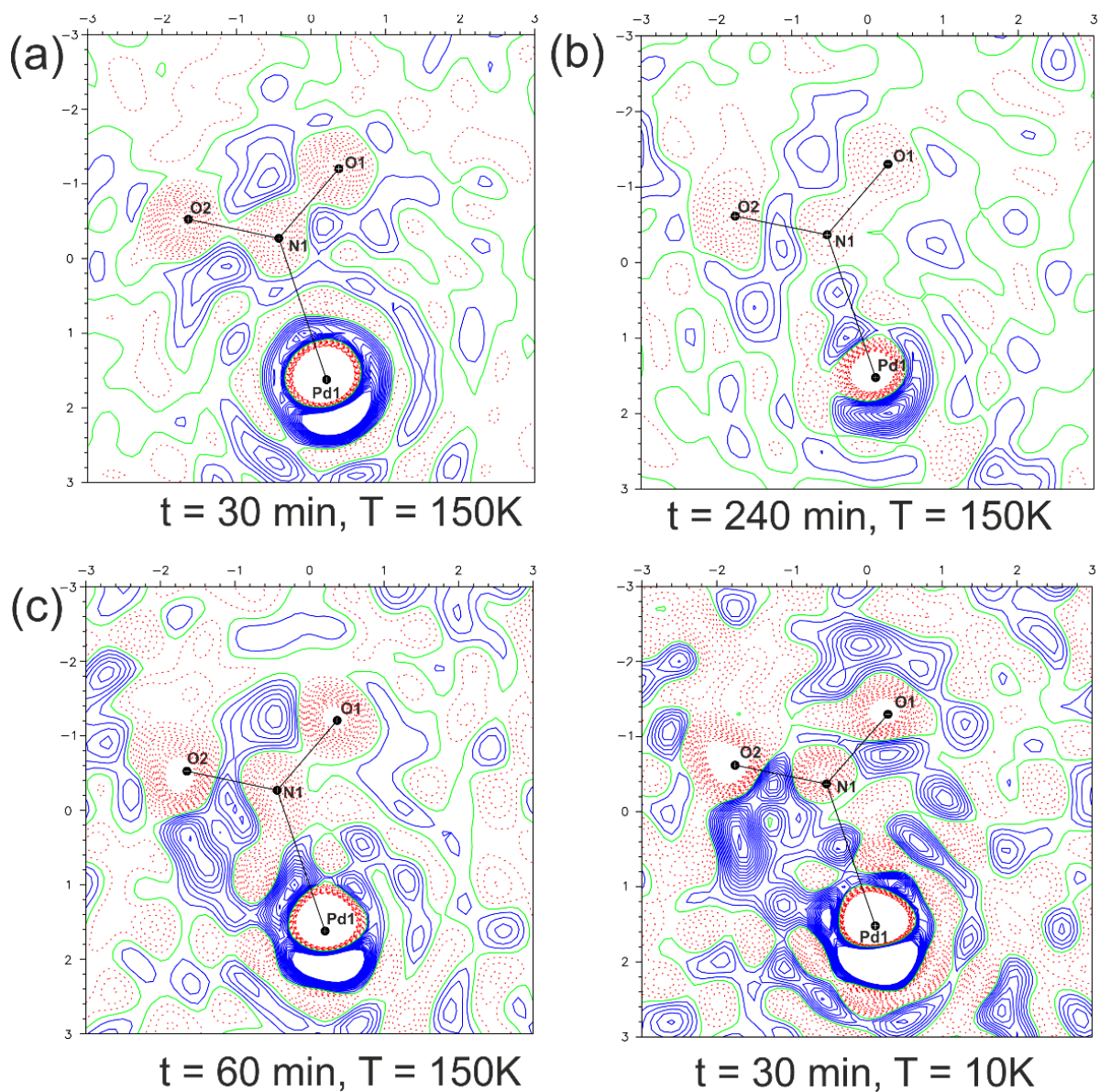


Fig. S1. Photodifference maps between photoexcited (a) Co, (b) Rh and (c) Cr, and corresponding ground state data expressed as $F_{\text{obsPLI}} - F_{\text{obsGS}}$ at given temperature and irradiation time. Contour level is equal to $0.5 \text{ e}/\text{\AA}^3$. [1] The 2D maps gives just approximate view of the disorder, since photoexcited ONO groups do not lie perfectly in O1-N1-O2 plane.

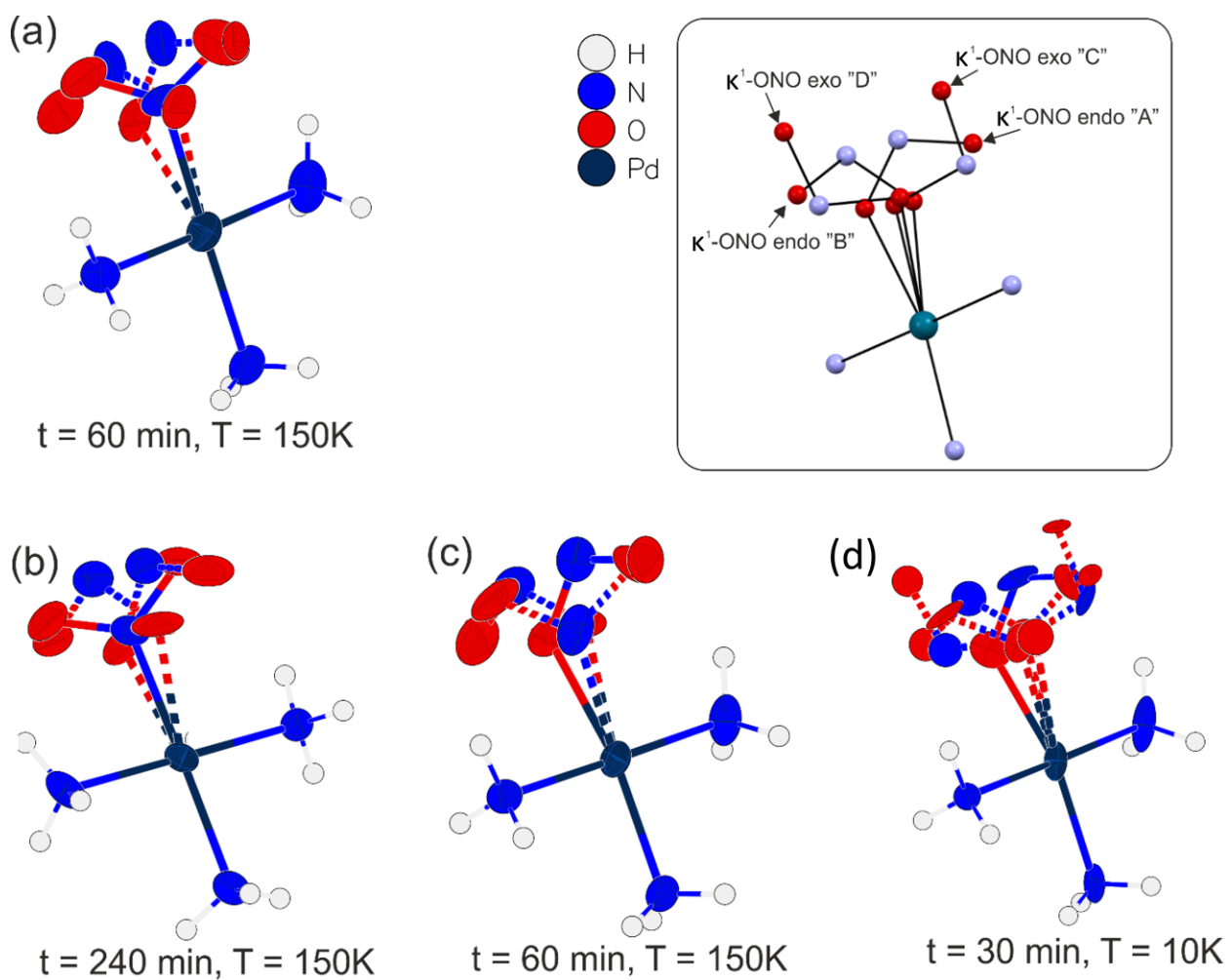


Fig. S2. The X-ray structures of PLIs of **Co** (a), **Rh** (b) and **Cr** (c, d) at given temperature and irradiation time. ADP's were drawn at 50% probability level. For clarity only photoreactive units are shown. [2]

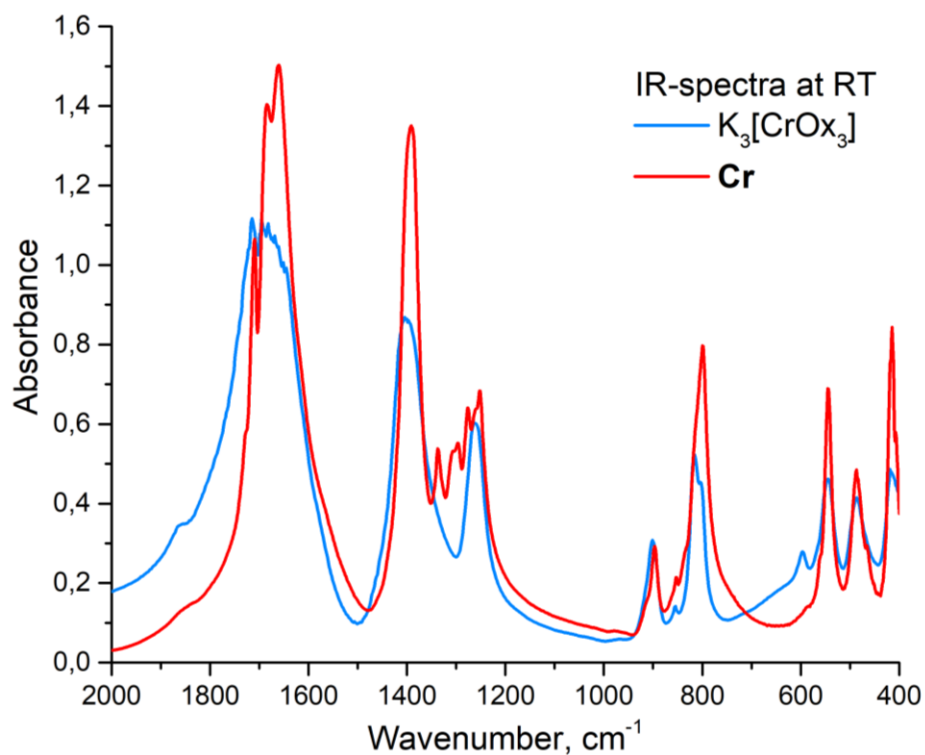


Fig. S3. Comparison of IR-spectra of $[Pd(NH_3)_4][Pd(NH_3)_3NO_2][CrOx_3]$ (Cr) and its precursor $K_3[CrOx_3]$ at room temperature (RT).

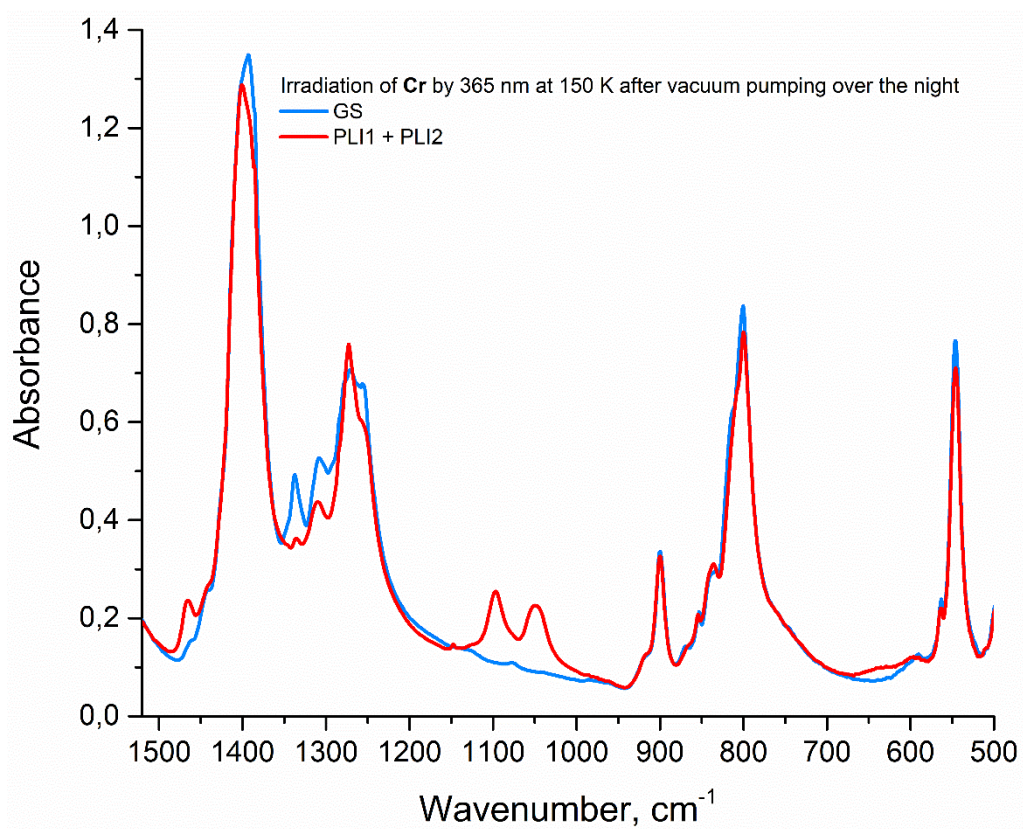


Fig. S4. IR-spectra of Cr at 150 K before (GS) and after (PLI1 + PLI2) light irradiation by 365 nm after vacuum pumping over the night.

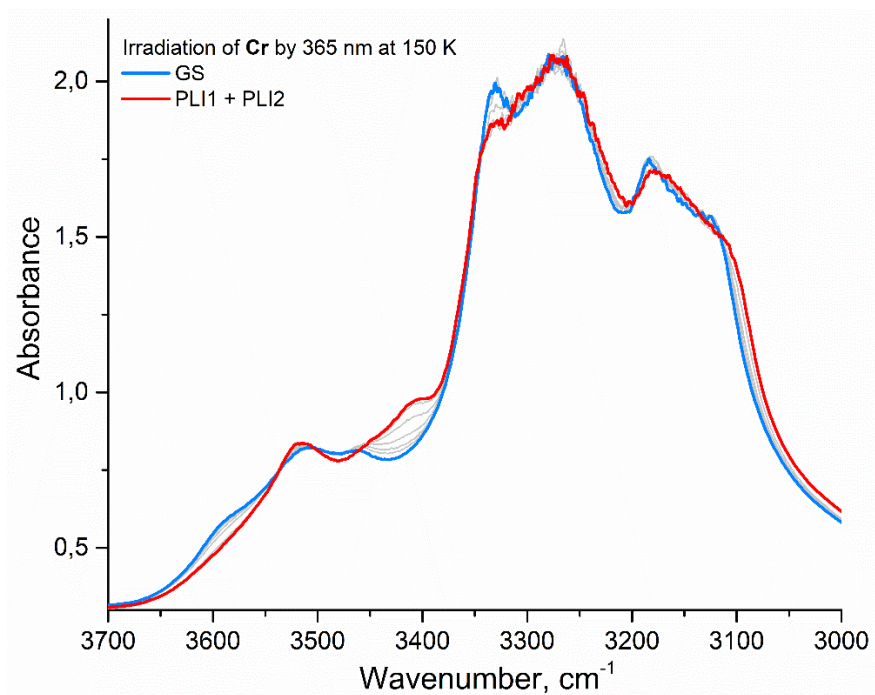


Fig. S5. IR-spectra of Cr at 150 K before (GS) and after (PLI1 + PLI2) light irradiation by 365 nm.

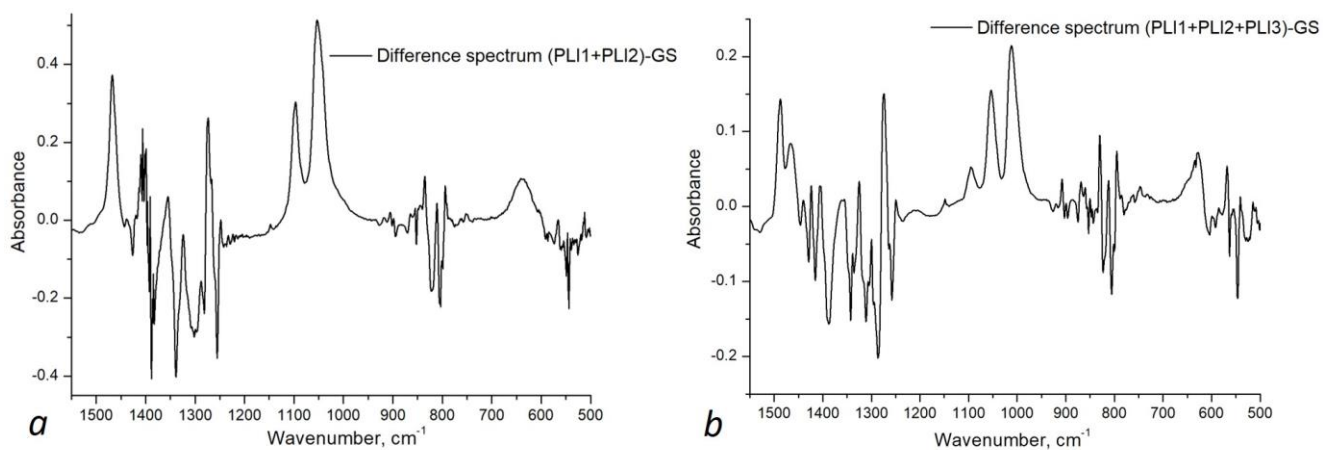


Fig. S6. Difference IR-spectra of Cr at 150 K (panel *a*) and 10 K (panel *b*) before and after light irradiation at 365 nm.

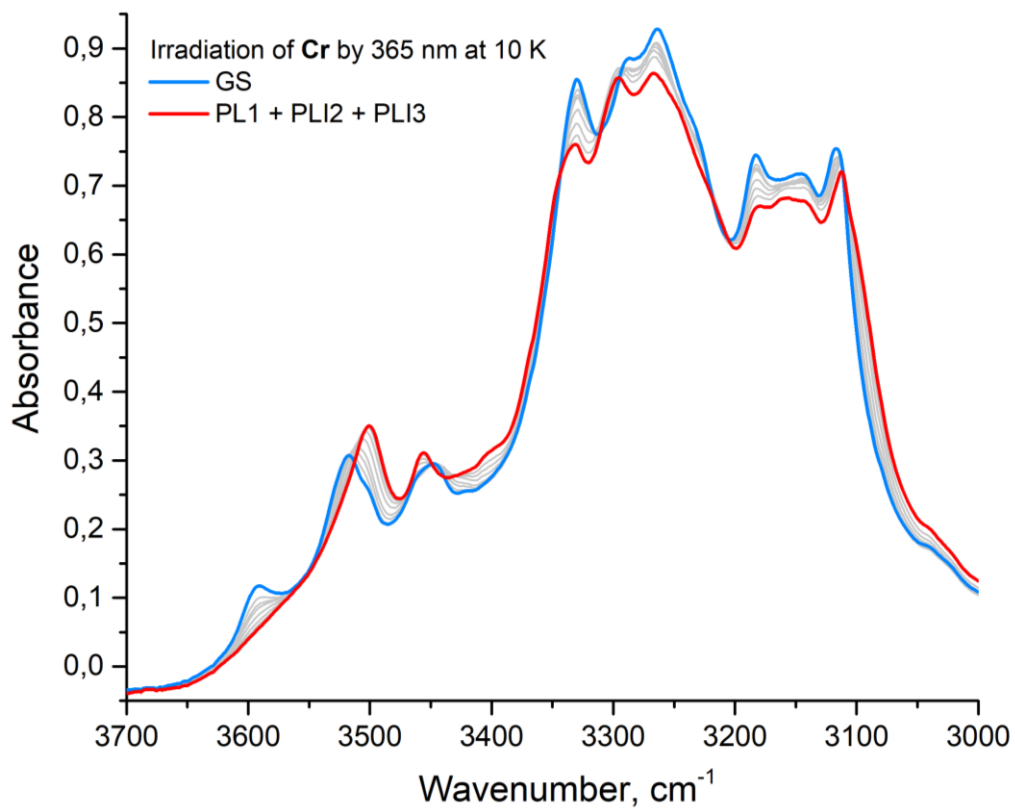


Fig. S7. IR-spectra of **Cr** at 10 K before (GS) and after (PLI1+ PLI2 + PLI3) light irradiation by 365 nm.

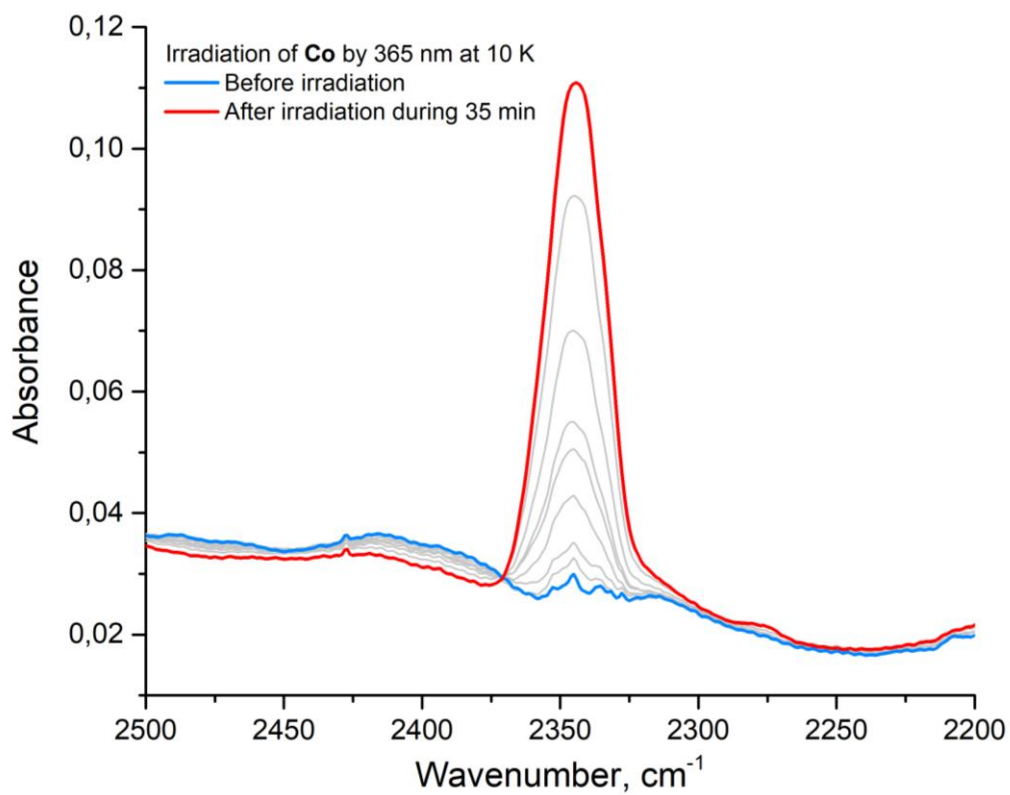


Fig. S8. IR-spectra of **Co** at 10 K before and after light irradiation by 365 nm.

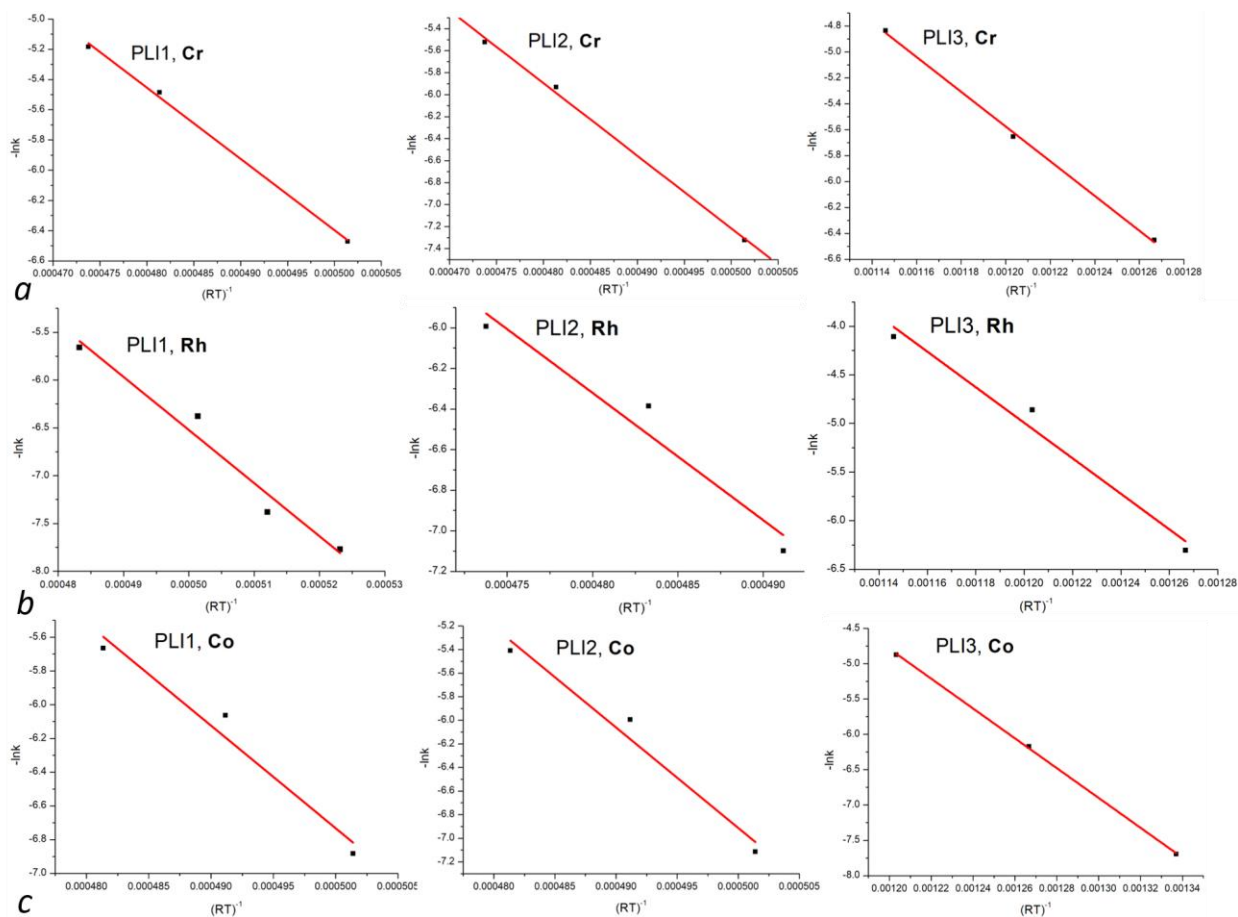


Fig. S9. Arrhenius plots of the reactions of thermal decay of PLI1-3 in **Cr** (*a*), **Rh** (*b*) and **Co** (*c*).

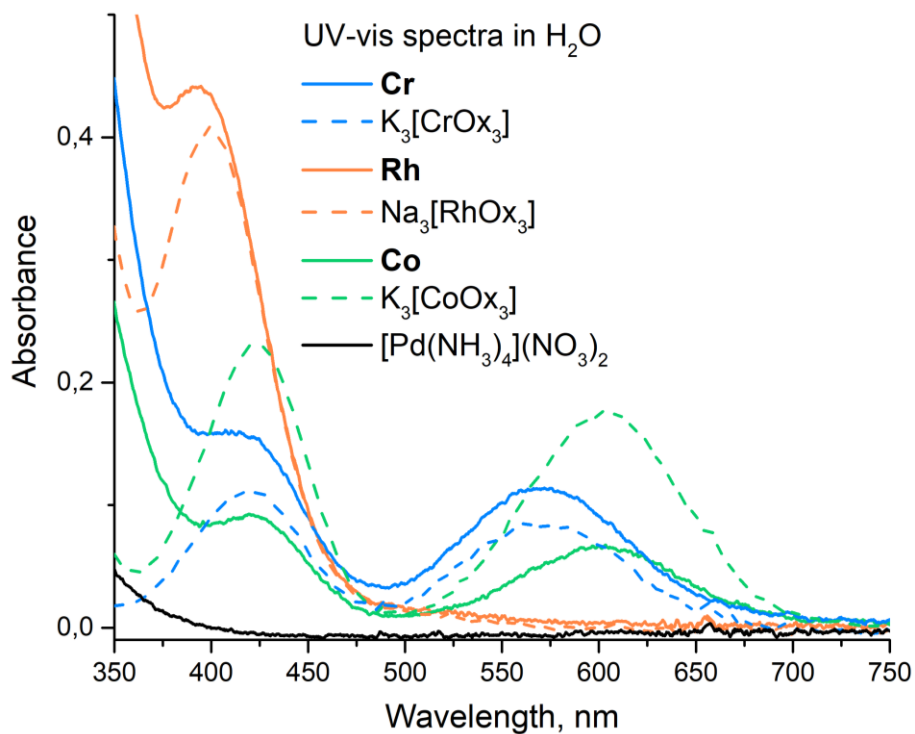


Fig. S10. UV-vis-spectra in water of $\approx 10^{-3}$ M solutions of **Cr**, **Rh**, **Co**, corresponding oxalate salts and $[Pd(NH_3)_4](NO_3)_2$.

References

- [1] L.J. Farrugia, WinGX and ORTEP for Windows: An update, *J. Appl. Crystallogr.* 45 (2012) 849–854. <https://doi.org/10.1107/S0021889812029111>.
- [2] O. V. Dolomanov, L.J. Bourhis, R.J. Gildea, J.A.K. Howard, H. Puschmann, OLEX2: A complete structure solution, refinement and analysis program, *J. Appl. Crystallogr.* 42 (2009) 339–341. <https://doi.org/10.1107/S0021889808042726>.